

# <sup>1</sup> Chapter 1

## <sup>2</sup> Experimental results

### <sup>3</sup> *Diamond irradiation study*

<sup>4</sup> This chapter contains the measurement results of data taken with diamond sensors.  
<sup>5</sup> First the measurement setup is described (section 1.1). Then the measured particle  
<sup>6</sup> spectra are shown in 1.2. This is followed by a study of effects of irradiation damage  
<sup>7</sup> on the electrical signal of the diamond detector and its lifetime. The last section  
<sup>8</sup> shows the results of the measurements of irradiated diamond samples at cryogenic  
<sup>9</sup> temperatures. The aim of these studies is to find the operational limitations of dia-  
<sup>10</sup> mond detectors for spectroscopy and tracking applications. The studies compare the  
<sup>11</sup> experimentally acquired data with the theory from the previous chapter and define  
<sup>12</sup> limitations of the diamond detectors in terms of noise, radiation and temperature.

<sup>13</sup> Diamond sensors are mainly used for two types of measurements: particle counting  
<sup>14</sup> and spectroscopy. The first type of measurements depends on the sensor efficiency –  
<sup>15</sup> its ability to detect all or at least a known percentage of incident particles. The energy  
<sup>16</sup> of the particles is not so important; what bears the information is the rate and the  
<sup>17</sup> spatial distribution. Here the particles do not necessarily stop in the bulk, but rather  
<sup>18</sup> continue their way. In spectroscopy, on the other hand, the particles stop within the  
<sup>19</sup> sensor, depositing all their energy. This energy is then measured by collecting the  
<sup>20</sup> freed charge carriers. The aim of the experiments described in this chapter is to:

- <sup>21</sup> 1. Quantify the efficiency of the sCVD diamond in counting mode,
- <sup>22</sup> 2. Quantify the degradation of efficiency as a function of the received radiation  
dose,
- <sup>24</sup> 3. Quantify the macroscopic effects on charge carrier behaviour as a function of  
the received radiation dose and
- <sup>26</sup> 4. Define limitations for use in spectroscopy.

<sup>27</sup> The results discussed here show that there are several limitations for using diamond  
<sup>28</sup> as a measurement device. All of them need to be taken into account when designing  
<sup>29</sup> a new measurement device. The first step is to build a setup that is insensitive to

## 1.1. MEASUREMENT SETUP

---

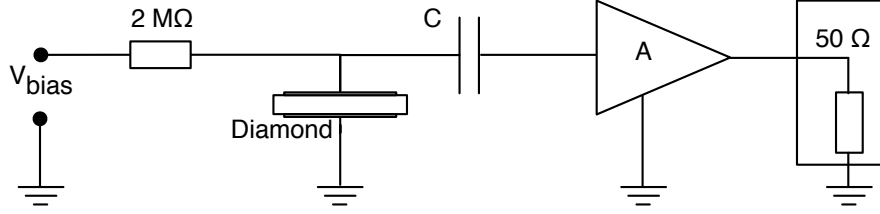


Figure 1.1: Diagram of a diamond detector readout chain.

30 external electromagnetic interferences and minimises electrical noise in the system.  
31 The setup needs to be calibrated before use. Then the measurement conditions have to  
32 be defined, such as the temperature, the type of radiation and its flux. This allows for  
33 an estimation of the lifetime of the detector and a prediction of the longterm signal  
34 degradation as a function of the dose. The degraded signal can then be corrected  
35 during data analysis.

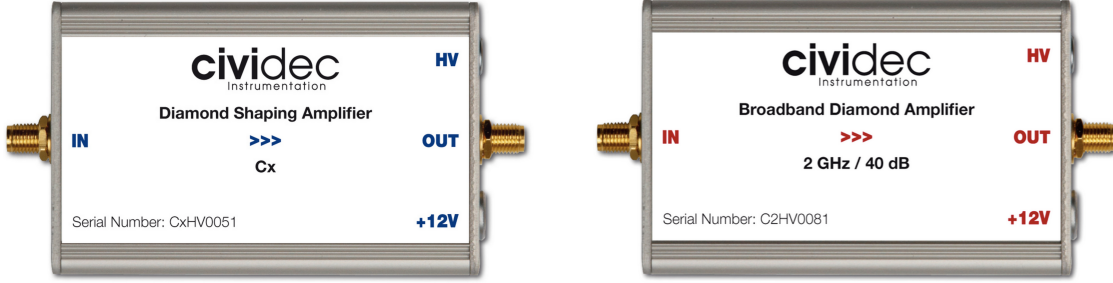
### 36 1.1 Measurement setup

37 A measurement setup has to be designed to minimise noise. Shielding has to be  
38 applied wherever possible. For instance, aluminium foil can be wrapped around  
39 the exposed parts of the system to shield them from external radio-frequency (RF)  
40 interferences. In addition, the sensors have to be covered to prevent the light from  
41 shining directly onto them. The incident photons can deposit enough energy to  
42 increase the leakage current of the detector, which produces unwanted results.

43 The measurements using diamond that are explained in these chapters have been  
44 carried out using several measurement setups, but they are all similar in terms of  
45 the electrical signal chain. The measurement chain consists of three main parts: a  
46 diamond sensor, a signal preamplifier and a readout device, as seen in figure 1.1. The  
47 signals propagating along the analogue chain are fast – in the GHz bandwidth range  
48 – and with low amplitudes – of the order of tens of  $\mu\text{V}$ . This gives rise to importance  
49 of RF shielding. Also, the connection between the carrier and the preamplifier has  
50 to be as short as possible to avoid capacitive signal losses in the transmission line.  
51 Finally, the system needs to be grounded properly.

#### 52 1.1.1 Preamplifiers

53 Two preamplifiers are used for the measurements, one sensitive to charge and the  
54 other to current. *CIVIDEC Cx* (figure 1.2a) is a charge sensitive amplifier. Its high  
55 SNR due to a low equivalent noise charge of  $300 + 30 \text{ pF}^{-1} \text{ e}^-$  and a reported gain  
56 of  $\sim 12 \text{ mV/fC}$  makes it a good choice for spectroscopic measurements with diamond  
57 sensors. *CIVIDEC C2* (figure 1.2b) is a fast current preamplifier with a 2 GHz  
58 bandwidth limit. It is used for TCT measurements because if its fast response and



(a) Cx charge sensitive preamplifier. (b) C2 fast charge preamplifier.

Figure 1.2: Amplifiers used for the charge and current measurements.

59 a good SNR. Both are embedded in an RF-tight aluminium box to reduce the noise  
60 pickup. Both have an AC coupled input and an output with a  $50\ \Omega$  termination.

## 61 Calibration

62 The amplifiers have to be calibrated before use to determine their gain. Both are  
63 calibrated using a square signal generator with a known amplitude step of  $U_{\text{in}} =$   
64  $(252 \pm 5)$  mV. A 2 GHz oscilloscope with a 10 GS/s sampling is used to carry out  
65 these measurements.

66 In the case of the Cx charge sensitive amplifier, the signal is routed through a  
67 capacitor with a calibration capacitance  $C_{\text{cal}} = (0.717 \pm 0.014)$  pF and then to the  
68 input of the amplifier. The pulse area behind the capacitor is  $a_{\text{cal}} = (5.0 \pm 0.5)$  pVs,  
69 with the signal amplitude on the output amounting to  $U_{\text{Cx}} = (1.95 \pm 0.05)$  V. The  
70 input voltage step combined with the calibration capacitance yields a calibration  
71 charge  $Q_{\text{cal}} = C_{\text{cal}} \cdot U_{\text{in}} = (181 \pm 5)$  fC. The gain of the Cx amplifier is therefore  
72  $A_{\text{Cx}}^Q = \frac{U_{\text{Cx}}}{Q_{\text{cal}}} = (9.3 \pm 0.4)$  mV/fC or  $A_{\text{Cx}}^a = \frac{U_{\text{Cx}}}{a_{\text{cal}}} = (390 \pm 40)$  mV/pVs. The area-based  
73 amplification factor has a higher uncertainty ( $\sim 10\%$ ) than the amplitude-based  
74 factor ( $\sim 4\%$ ) due to the measurement limitations of the oscilloscope. Nevertheless,  
75 it can be used as an estimate for the integrated charge of a current pulse.

76 To calibrate the C2 current amplifier, only the amplitude gain has to be measured.  
77 The input signal amplitude has to be such that it keeps the output amplitude within  
78 the amplifier's linear range, that is  $\pm 1$  V. The signal from the generator is therefore  
79 routed through a 36 dB attenuator to decrease its amplitude to  $U_{\text{inAtt}} = (3.95 \pm$   
80  $0.05)$  mV. Two amplifiers with different gains have been measured, because both are  
81 used for the measurements. The output of the first amplifier amounts to  $U_{\text{C2-1}} =$   
82  $(860 \pm 5)$  mV. This yields the amplification gain equal to  $A_{\text{C2-1}} = \frac{U_{\text{inAtt}}}{U_{\text{C2-1}}} = (217 \pm 3)$ .  
83 The second amplifier has the output equal to  $U_{\text{C2-2}} = (632 \pm 5)$  mV with the resulting  
84 gain of  $A_{\text{C2-2}} = (152 \pm 3)$ .

## 1.1. MEASUREMENT SETUP

---

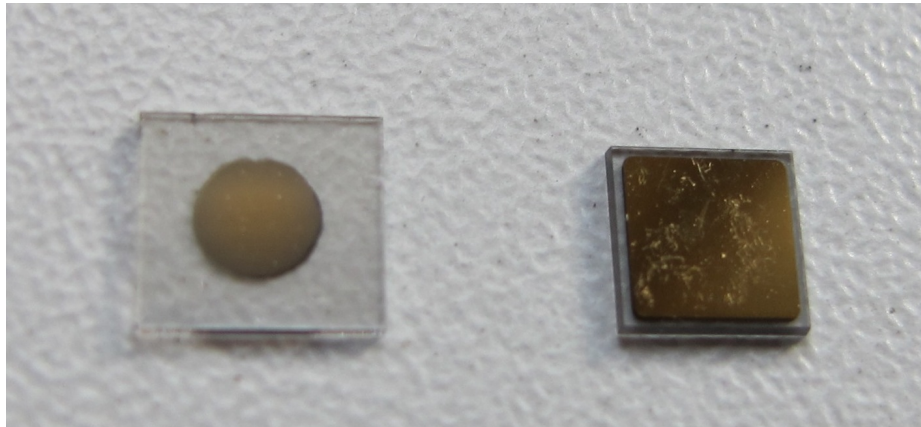


Figure 1.3: Two scCVD diamond samples: A IIa 1scdhq (left) and an E6 S37 (right).

### 1.1.2 Diamond samples

Detector-grade diamonds are very difficult to produce, mostly because it is very difficult to ensure a high enough purity of the lattice. The sensor samples used for these studies have been bought at Element Six (E6) [?]. They all have the same standard dimensions. sCVD diamonds with dimensions  $4.7 \times 4.7 \text{ mm}^2$  are already sufficiently large for most of the beam monitoring applications and still affordable. One of the samples with dimensions of  $5.6 \times 5.3 \text{ mm}^2$  produced by IIa Singapore [?] has also been sent to CERN to be characterised. The target thickness for all the samples is 500  $\mu\text{m}$ . Diamonds this thick yield a high enough signal-to-noise ratio for MIPs to be measured by the available electronics. Table 1.1 shows all the samples used for this study. Two of them are measured before and after irradiation with 300 MeV pions and then compared. Irradiation doses for damaging the material need to be high – above  $10^{12}$  particles per  $\text{cm}^2$  to be able to observe a significant change in behaviour of a diamond sensor.

99	Name	Type	Producer	Dimensions [ $\text{mm}^2$ ]	Thickness [ $\mu\text{m}$ ]	Electrode	Irradiated
100	S37	sCVD	E6	$4.7 \times 4.7$	548	Cr/Au	no
	S50	sCVD	E6	$4.7 \times 4.7$	537	Cr/Au	no
	S52	sCVD	E6	$4.7 \times 4.7$	515	Cr/Au	$1 \times 10^{14} \pi \text{ cm}^{-2}$
	S79	sCVD	E6	$4.7 \times 4.7$	529	Cr/Au	$3.63 \times 10^{14} \pi \text{ cm}^{-2}$
	ELSC	sCVD	E6	$4.7 \times 4.7$	491	Cr/Au	no
	1scdhq	sCVD	IIa	$5.6 \times 5.3$	460	Cr/Au	no

101 Table 1.1: Diamond sensor samples used.

102 The diamond samples have quoted impurity densities of  $\leq 2 \times 10^{14} \text{ cm}^{-3}$  and  
103 nitrogen incorporation of  $\leq 1 \text{ ppb}$ . The electrodes were added by various companies  
104 and institutes. For instance, S52 was metallised by a company DDL (now defunct)  
105 while the Physics Department of the University of Firenze, Italy metallised the S79.  
106 There are also several techniques for producing the electrodes. The DDL contacts

107 consist of three layers: DLC (diamond-like carbon)/Pt/Au with 4/10/200 nm thick-  
108 nesses, respectively. The metallisation for S79, on the other hand, is made up of  
109 Cr/Au with a total thickness of  $\sim$ 400 nm. The area coverage also differs from sample  
110 to sample. Diamonds must not be metallised until the very edge as the proximity of  
111 contacts with a high potential may lead to sparking. However, the areas not covered  
112 by the metallisation are less efficient because the fringe fields at the edges are not  
113 as strong as in between the electrodes. This effectively reduces the sensitive area of  
114 the sensors. In the diamonds used here the effective area is anywhere from 9 mm<sup>2</sup> to  
115 18 mm<sup>2</sup>. The leakage current through the bulk is below 1 ns, but increases for the  
116 irradiated samples. The capacitance is of the order of (2.0 $\pm$ 0.3) pF.

### 117 1.1.3 Readout devices

118 Electrical signals in diamond detectors are in the GHz frequency range. To preserve  
119 the information in the signals, the readout device with a high bandwidth limit must  
120 be used. For instance, a 250 MHz limit is enough for the spectroscopic measurements  
121 with the Cx charge amplifier, but might be insufficient for the current measurements  
122 with the C2 amplifier.

123 Two devices are used take data shown in this chapter. The first choice is a 2 GHz  
124 LeCroy WaveRunner 204MXi-A. This specific model has a sufficiently high bandwidth  
125 limit for the fast current preamplifier signals. It offers a versatile solution for analogue  
126 signal readout – fast to set up and reliable, hence convenient for use in laboratory tests  
127 and for experiments where limited amounts of data are taken and where speed is not  
128 crucial. However, its slow acquisition speed is a bottleneck in a test beam experiment.  
129 Its initial 100 Hz readout rate decreases to a mere 20 Hz within 20 minutes, because  
130 every single trigger is saved as a separate file and the Windows operating system  
131 is not capable of handling 10000+ files in a single directory easily. This is why it  
132 has been exchanged with a DRS4 [?], an analogue readout device developed by PSI,  
133 Switzerland. This compact device is capable of recording up to four waveforms at a  
134 time at a steady rate of up to 500 Hz. Its 700 MHz bandwidth limitation is sufficient  
135 for the signal from the charge amplifier.

### 136 1.1.4 Setup for the efficiency study using $\beta$ particles

137 The efficiency study of the diamond sensors has been carried out at CERN in the  
138 North Hall test beam facility. There a straight high-energy particle beam of  $\pi_{120\text{ GeV}}$  is  
139 provided to the users to calibrate their detectors. The beam has a transverse spread  
140 of  $\sigma = 10$  mm in both axes. The particle rate is of the order of  $10^4 \pi \text{ cm}^{-2} \text{ s}^{-1}$ .  
141 A diamond sensor embedded in a PCB carrier has been placed in the beam spot  
142 perpendicular to the beam and connected via an SMA connector directly to a charge  
143 amplifier. The amplified signal is read out using a LeCroy oscilloscope and a DRS4  
144 analogue readout system. A computer is used as a controller and data storage for  
145 the readout device. A beam telescope is used as a reference detector. It is a device

## 1.1. MEASUREMENT SETUP

---

that helps to cross-check the measurements of the devices under test (DUTs) and to carry out spatially resolved studies on the DUTs. It consists of several pixellated sensor planes placed in series, which can track a particle's trajectory with a precision of a few  $\mu\text{m}$ . The sensor planes are positioned in front of the DUT and behind it. Then the beam telescope acts as a trigger system – it triggers the readout of both the telescope data and DUT data when both the planes in front and behind the DUT record a hit by an incident particle. A particle detected by all the planes within the DUT window and the DUT itself counts towards its efficiency whereas a hit missed by the DUT means that the DUT is not 100 % efficient. To discard the hits that miss the DUT completely, a region of interest (ROI) can be chosen in the beam telescope planes. The equation for calculating the sensor efficiency is therefore

$$\epsilon = \frac{N_{\text{DUT}} \wedge N_{\text{telescope}}}{N_{\text{telescope}}} \quad (1.1)$$

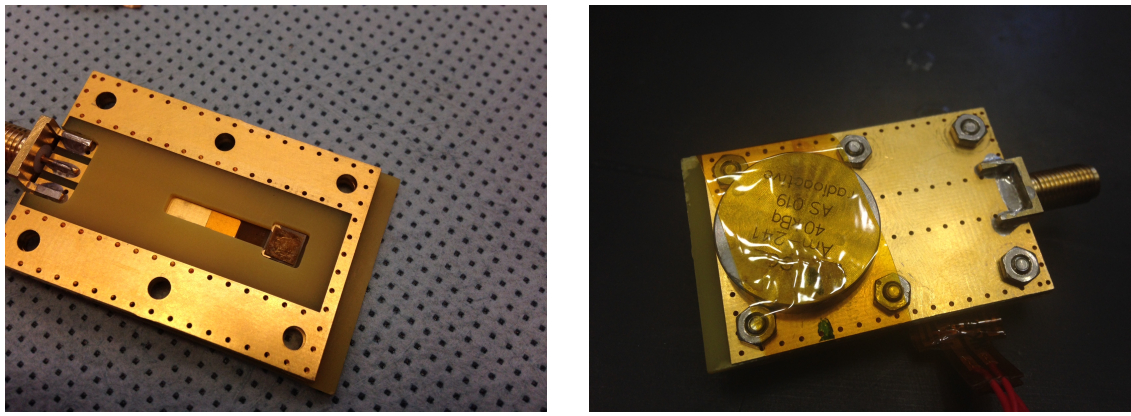
for an ROI smaller than the sensitive region of the diamond.

### 1.1.5 Room temperature $\alpha$ -TCT setup

This TCT study is a follow-up of an extensive diamond TCT study at cryogenic temperatures [?]. The room-temperature TCT measurements have been carried out in the laboratory. The setup consists of a diamond sensor embedded in a PCB carrier, a current amplifier and an oscilloscope. To measure  $\alpha$  particles, their energy loss during their trajectory has to be minimised. Therefore the diamond is placed inside a vacuum chamber. The chamber is a steel tube with a diameter of 5 cm. On one side it is connected to a vacuum pump via a steel hose. A feedthrough with an SMA connector is placed on the other side. A C2 current amplifier is connected directly onto the feedthrough. The amplified output is connected to the oscilloscope via an SMA cable. An  $^{241}\text{Am}$  source with a diameter of 2 cm and a height of 0.5 cm is fixed onto the sensor carrier (figure 1.4a, figure 1.4b). Then the carrier is inserted in the chamber and fixed in place using an air-tight clamp. The pump can then be switched on. It is capable of providing the inside pressure as low as  $10^{-4}$  mbar after approximately one hour of operation, but measurements can take place even after five minutes of evacuation, at around  $10^{-3}$  mbar. The most important thing is to switch the bias voltage of the sensor OFF during the process of evacuation. This is due to gas becoming more conductive at the pressure of the order of  $10^{-1}$  mbar, which is at the bottom of Paschen's curve [?]. A failure to switch the bias voltage off may cause a spark between the signal and ground line, destroying the amplifier.

### 1.1.6 Cryogenic $\alpha$ -TCT setup

The experiment at cryogenic temperatures has been carried out in the Cryolab at CERN. The room-temperature TCT setup has to be modified to allow for measurements at temperatures as low as 2 K. It consists of three parts:



(a) PCB carrier with an embedded diamond sample.  
(b) Radioactive source over the carrier.

Figure 1.4: Positioning of the  $\alpha$ -source on top of the sensor carrier.

- 182 1. a cryostat – a thermally insulated cylinder containing liquid helium,  
183 2. an inlet – an air-tight mechanical tube with valves and feedthroughs at the top  
184 that is lowered in the liquid helium and  
185 3. the diamond sample embedded in a PCB carrier with a fitted temperature  
186 sensor, a heater and cables leading to the feedthroughs.

187 The setup is described in detail in [?].

188 When the diamond sample is placed in the PCB carrier and the  $^{241}\text{Am}$  source is in  
189 place, the inlet is sealed and lowered in the empty cryostat. Then the inside volume  
190 of the inlet is evacuated down to  $10^{-5}$  mbar while the liquid helium is flowing into  
191 the cryostat. To improve the thermal contact between the diamond and the coolant,  
192 a small amount of helium gas is added inside the evacuated inlet, setting the vacuum  
193 to around  $10^{-3}$  mbar. This value changes with time, because the gas condenses on  
194 the walls of the inlet, reducing the number of floating particles. For this reason the  
195 helium gas has to be added on an irregular basis. Every addition causes a significant  
196 undershoot of the sample temperature, which has to be corrected for using a heater  
197 placed on the back of the PCB carrier. Also, the added gas deteriorates the vacuum  
198 inside the inlet. It is very important to monitor the pressure so as not to let it rise  
199 above  $10^{-2}$  mbar. The gas at this pressure is significantly more conductive and can  
200 cause a short circuit between the two diamond plates or in the SMA connectors,  
201 destroying the amplifier. Furthermore, at approximately 60 K the helium gas has to  
202 be evacuated from the inlet to avoid a potential explosion due to the expansion of  
203 the gas with temperature.

204 When the sample is cooled to the minimum temperature achievable by means of  
205 liquid helium without over-pressurising it (4.2 K), the measurements can begin. A  
206 temperature sensor placed on the back of the PCB carrier is used to measure the  
207 temperature of the sample. After every temperature data point, the current through

208 the heater placed in the PCB next to the diamond sample is increased, increasing the  
209 sample. The initial temperature time constant of the order of tenths of seconds at low  
210 temperatures increases with temperature. Even more so when helium is evacuated  
211 from the inlet at 60 K, removing the thermal bridge between the wall of the inlet and  
212 the diamond sample. At the room temperature (RT), the time constant is already of  
213 the order of minutes.

## 214 1.2 Charged particle pulses and spectra

215 In previous chapter the ionisation profiles for different types of radiation were dis-  
216 cussed. It is known that  $\beta$  and  $\gamma$  radiation induces a triangular electric pulse whereas  
217  $\alpha$  radiation induces a rectangular one. However, their amplitude, width and rise/fall  
218 time depend heavily on the type of interaction with the diamond, the purity of the  
219 diamond and the bandwidth of the amplifier and the oscilloscope. This section shows  
220 the signal pulses of  $\alpha$ ,  $\beta$  and  $\gamma$  radiation with their respective energy distributions for  
221 the case of a diamond detector. This is followed by a discussion of effects of noise on  
222 these measurements.

223 A CIVIDEC C2 current amplifier together with the LeCroy oscilloscope (both  
224 with a bandwidth limit of 2 GHz) is used to record the pulse shapes whereas the Cx  
225 charge amplifier is used for charge measurements. A 2 GHz bandwidth limit defines  
226 the minimum rising time equal to  $t_r \simeq \frac{0.34}{BW} = \frac{0.34}{2 \times 10^9} = 170$  ps, therefore the system is  
227 capable of measuring pulses with a minimum FWHM  $\simeq 170$  ps. This already makes it  
228 impossible to measure the initial peak in the  $\alpha$  response due to the two opposite charge  
229 carriers travelling. If a charge carrier travelling through the bulk takes  $t_{t1} \sim 6$  ns to  
230 reach the electrode on the opposite side ( $d_1 \sim 500$   $\mu\text{m}$ ), the carrier with the opposite  
231 charge and a shorter path to the closer electrode – max.  $d_2 \sim 10$   $\mu\text{m}$  – only takes  
232  $t_{t2} \sim \frac{d_2}{d_1} t_{t1} = 120$  ps. A drift time this short induces a current pulse that is too narrow  
233 for the C2 amplifier or the oscilloscope to be able to observe.

234 Figure 1.5 shows a set of pulses and an averaged pulse for  $\alpha$ ,  $\beta$  and  $\gamma$  radiation  
235 using an  $^{241}\text{Am}$ ,  $^{90}\text{Sr}$  and  $^{60}\text{Co}$  source, respectively. The particles are measured with  
236 the non-irradiated sCVD diamond S37.  $\alpha$  particles always produce the same signal  
237 pulse, but with a high noise RMS. The averaging suppresses the noise while retaining  
238 most the information. It does, however, smear the rising and falling edge, increasing  
239 the rising and falling time. The  $t_r$  is now of the order of 0.5 ns. Both  $\beta$  and  $\gamma$  pulses  
240 look similar - triangular and with a wide range of amplitudes. Here the pulse count  
241 is low, so the pulses with a high amplitude are not recorded. A trigger set very high  
242 would be needed to “catch” them with the oscilloscope.

### 243 1.2.1 Noise limitations

244 Noise is a major limiting factor in particle detection. It defines the minimum measur-  
245 able particle energy and the minimum measurement resolution. It is hence important  
246 to minimise the electric noise in the detector signal. The major noise contribution

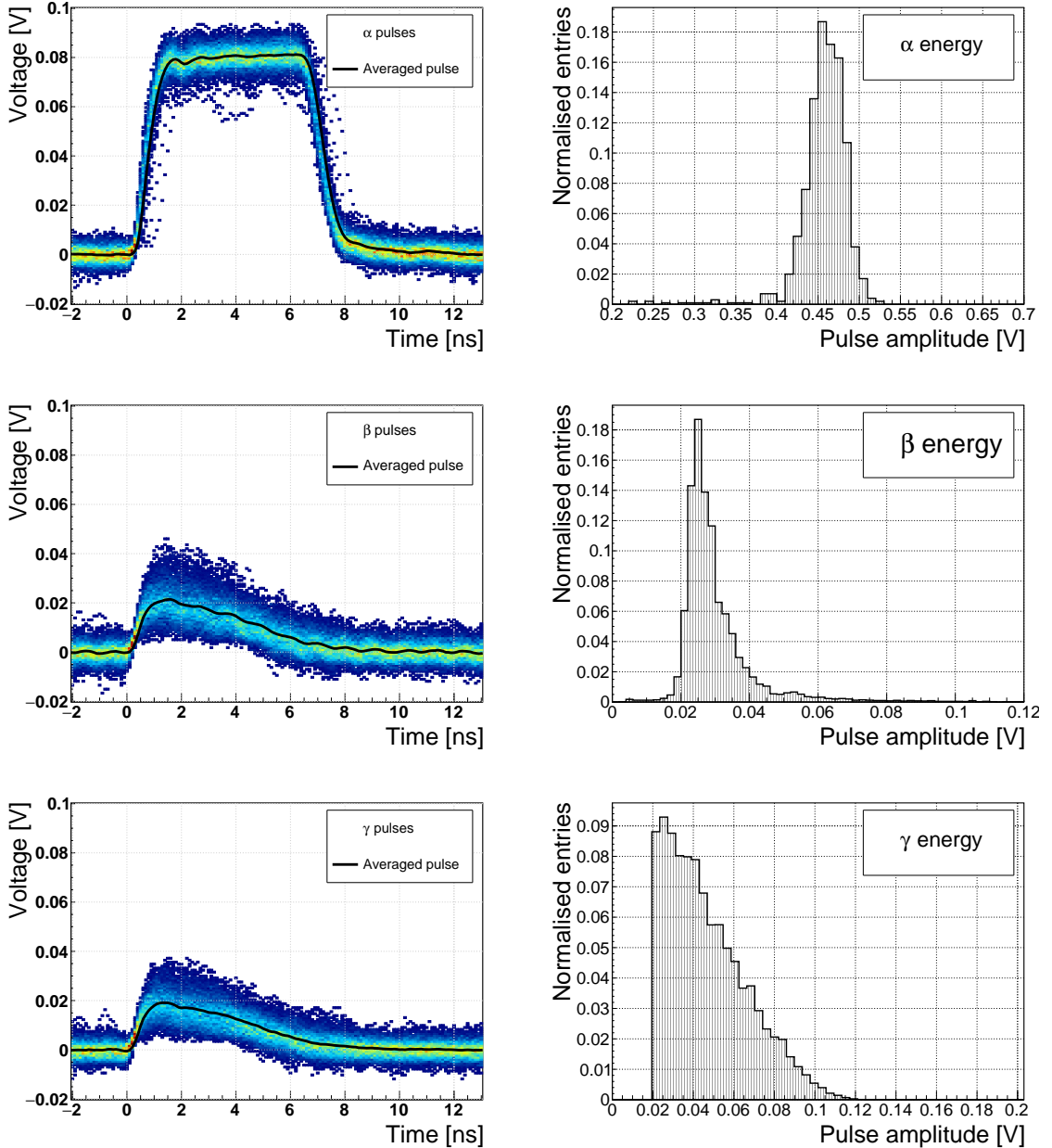


Figure 1.5: Superimposed and averaged pulses (left figures, current amplifier) and distributions of deposited energy (right figures, charge amplifier) for three types of radiation. Note the scale on the X axis of the distributions.

comes from poor shielding from external electromagnetic sources. These often cause ringing whereby the signal oscillates with a frequency defined by the external source. The ringing makes high-frequency measurements impossible. Another source of noise is the sensor itself. In the case of silicon, natural light increases the number of thermally excited free charge carriers, increasing the leakage current. This is not the case for diamond, which is with its high energy band gap insensitive to visible light.

### 1.3. RADIATION LIMITATIONS

---

253 Nevertheless, any noise produced by the sensors is amplified by the signal amplifiers, which add an additional noise of the analogue electrical circuit to the amplified  
254 signal. Finally, the digitisers add the quantisation noise to the digitised signal. If  
255 the measurement range is significantly higher than the actual measured signal, the  
256 quantisation noise can be a significant contributor to the decrease of the overall mea-  
257 surement resolution.  
258

## 259 1.3 Radiation limitations

260 Exposure to ionising radiation degrades sensors. It deforms the lattice by displacing  
261 the atoms. Various types of lattice defects can be created in diamond, similar to those  
262 in silicon: vacancies, interstitials etc. [?] These deformations introduce new discrete  
263 energy levels between the valence and conduction band. Charge carriers drifting in  
264 their vicinity can get trapped, their energy falling to the energy level of the trap.  
265 Their emission back to the conduction band depends on how deep the trap is (how  
266 far away from the conduction band it is). The carriers caught in the shallow traps  
267 of the order of 100 meV below the conduction band are excited back up already by  
268 means of thermal excitation. This phenomenon has a short time constant, dependant  
269 on the environmental temperature. Those stopped by deep traps near the middle  
270 of the band gap need more energy and thus more time to be emitted to either the  
271 conduction or valence band. Some charge carriers remain trapped for long periods.  
272 If they build up in a certain region of the diamond, their charge starts affecting the  
273 surrounding electric field – this is referred to as formation of space-charge. It can  
274 either help or counteract the field, depending on the polarity of the trapped carriers.

275 The energy band jumping goes the other way, too. The carriers in the valence band  
276 may use the intermediate energy levels as “stepping stones” to jump to the conduction  
277 band and start drifting in the externally applied electric field. This occurrence is  
278 referred to as the leakage current.

279 The electrons and holes stopped in these traps cause a decrease of the induced  
280 current on the electrodes. This yields a lower integrated charge in an irradiated  
281 sensor than that in a non-irradiated one. The charge collection efficiency is therefore  
282 correlated with the level of irradiation.

283 This section contains a study of the effects of pion ( $\pi_{300 \text{ MeV}}$ ) irradiation on the  
284 charge collection efficiency of sCVD diamond detectors. To carry out this study,  
285 two diamond samples have been irradiated to doses of  $1 \times 10^{14} \pi \text{ cm}^{-2}$  (S79) and to  
286  $3.63 \times 10^{14} \pi \text{ cm}^{-2}$  (S52). A test beam campaign has to be carried out to observe  
287 the charge collection efficiency at different bias voltage settings. The efficiency values  
288 acquired are used to determine the effective drop in efficiency with as a function of re-  
289 ceived radiation dose. This is to test if the collected charge  $Q$  is inversely proportional  
290 to the received dose  $\Phi$ . A procedure defined by a collaboration researching diamond  
291 behaviour RD42 has been applied to the measured values to extract the damage fac-  
292 tor. The next subsection contains measurements and results of a long-term stability  
293 study using  $\alpha$  and  $\beta$  particles. In particular, the charge collection efficiency as a

function of time is measured during the measurements with  $\beta$  and  $\alpha$  radiation. To investigate this effect on the scale of charge carriers, the change of TCT (transient current technique) pulses with time is observed. Finally, a procedure that improves the pulse shape and with it the charge collection is proposed.

### 1.3.1 Quantifying radiation damage in diamonds

Radiation damage varies with the type of radiation and its energy. There are several models existing [?, ?] that try to explain the impact of irradiation and to provide *hardness factors* to compare the radiation damage between different particles. The standard way is to convert the damage into *neutron equivalent* [?]. Some models have been extensively verified with simulations and with experiments. In these experiments the charge collection in sensors is measured before and after irradiation. This procedure is repeated several times, with a measurement point taken after every irradiation. When a set of measurements of charge collection is plotted against the radiation dose received by a specific particle at a specific energy, a damage factor  $k_\lambda$  can be extracted. Damage factors have to be measured across a range of energies and types of radiation to properly quantify the damage in the sensors. They are then compared against the simulations to verify that the experimental observations are in line with the theory.

Diamond is an expensive material and the technology is relatively new as compared to silicon. Therefore not many institutes are carrying out diamond irradiation studies. To join the efforts, the RD42 collaboration [?] has been formed. It gathers the experimental data from diamond irradiation studies. Unlike with silicon, the experimental results so far show no significant correlation with the NIEL (non-ionising energy loss) model [?], which correlates detector efficiency with the number of lattice displacements. Therefore an alternative model was proposed [?], correlating the diamond efficiency with the number of displacements per atom (DPA) in the bulk. The idea is that if the recoil energy of an incident particle is higher than the lattice binding energy (42 eV for diamond), the atom is displaced from its original position. The newly formed vacancy acts as a trap for drifting charge carriers. The more displacements that form in the bulk, the higher is the probability that a drifting carrier gets trapped. However, different types of particles interact differently with the bulk. In addition the mechanisms of interaction at low energies are different to those at high energies. To assess the damage for individual particles at a range of energies, simulations need to be run first. The simulation shown in [?] shows the DPA model for a range of energies of proton, pion and neutron irradiation in diamond. Figure 1.6 contains the simulation results as well as the superimposed empirical results of several irradiation studies. According to the figure, a 300 MeV pion beam damages the diamond bulk twice as much as a 24 GeV proton beam. The data points obtained by RD42 are also added to the figure. They have been normalised to damage by 24 GeV protons. Finally, the data point measured in the scope of this thesis has been added for comparison. The derivation is done below.

### 1.3. RADIATION LIMITATIONS

---

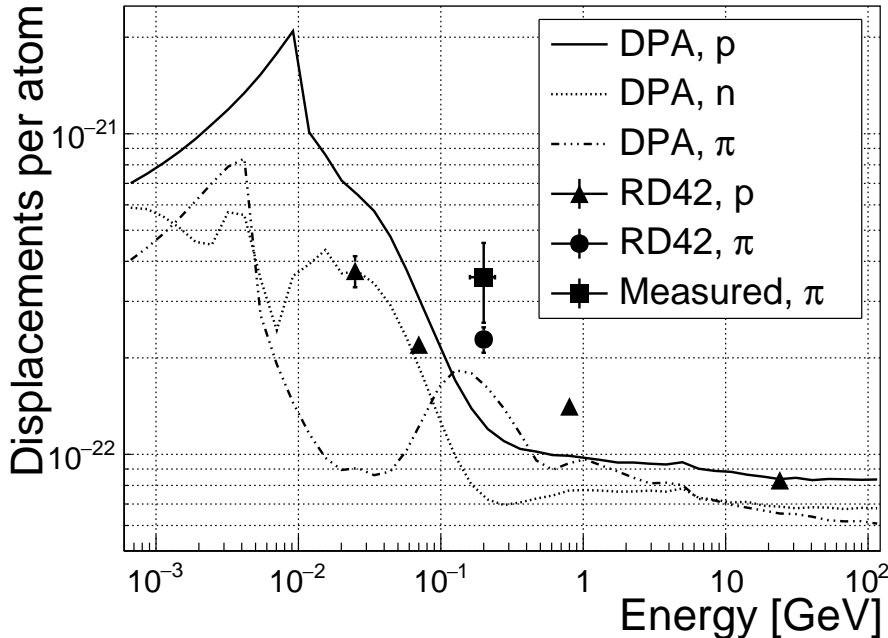


Figure 1.6: Diamond radiation damage - a model based on displacements per atom [?]. Added are data points for protons and pions by RD42 [?] and one data point for pions measured in the scope of this study.

335 **Irradiation with a  $\pi_{300 \text{ MeV}}$  beam**

336 The samples were irradiated at the Paul Scherrer Institute (PSI) [?] by means of a  
 337 beam of pions with an energy of 300 MeV (kinetic energy 191.31 MeV) and with a  
 338 flux of up to  $1.5 \times 10^{14} \pi \text{ cm}^{-2}$  per day. The system has a 10 % uncertainty on the  
 339 beam energy. In addition, their quoted uncertainty on the measurement has an error  
 340 of  $\pm 20 \%$ . Looking at the pion damage curve in figure 1.6,  $\pi_{300 \text{ MeV}}$  point sits on a  
 341 steep section of the DPA curve. This means that a deviation in beam energy can  
 342 have a significant effect on the damage.

343 Two diamond samples, S52 and S79, were put in the  $\pi_{300 \text{ MeV}}$  beam in the 2014  
 344 PSI irradiation campaign; S52 to  $(1 \pm 0.21) \times 10^{14} \pi \text{ cm}^{-2}$  and S79 to  $(3.63 \pm 0.77) \times$   
 345  $10^{14} \pi \text{ cm}^{-2}$ . During the process, the golden electrodes got slightly activated, but the  
 346 activation decayed in two weeks.

347 **Charge collection efficiency and charge collection distance**

348 Three diamonds – non-irradiated S37 and irradiated S52 and S79 – were tested in  
 349 a  $\pi_{120 \text{ GeV}}$  test beam in the SPS North Experimental Area at CERN [?] before and  
 350 after irradiation. The goal was to estimate the charge collection efficiency (CCE) and  
 351 charge collection distance (CCD) as a function of irradiation dose. The samples were  
 352 primed (pumped) prior to data taking using a  ${}^{90}\text{Sr}$  radioactive source. The data were  
 353 then taken at a range of bias voltages ranging from 30 V to 900 V, yielding between

354 0.06 V/ $\mu\text{m}$  and 1.8 V/ $\mu\text{m}$  electrical field in the bulk. Every data point contained  
355 approximately  $5 \times 10^4$  measured particles. The charge deposited by the particles  
356 was measured using a CIVIDEC Cx charge preamplifier. As expected, the integrated  
357 amplitude spectrum followed a landau distribution. Its most probable value (MPV)  
358 is used to calculate the most probable collected charge  $Q_i$ :

$$Q_i [e^-] = \frac{Q_i [fC]}{1.6 \times 10^{-4}} = \frac{MPV [mV]}{A [mV/fC]} \cdot 6.241 \times 10^4 \quad (1.2)$$

359 where  $A = 9.3 \text{ mV/fC}$  is the preamplifier gain factor. The CCD can then be calculated  
360 using the average number of electron-hole pairs produced per micrometer in diamond  
361  $\delta_d = 36 \text{ e-h } \mu\text{m}^{-1}$  (from table ??):

$$CCD = \frac{Q_i}{\delta_d}. \quad (1.3)$$

362 The resulting CCD for the three measured samples at bias voltages ranging from  
363 0.2–1.6 V  $\mu\text{m}^{-1}$  is shown in figure 1.7a. S37 exhibits a full collection distance already  
364 at 0.4 V  $\mu\text{m}^{-1}$  whereas the irradiated samples have a more gentle increase of CCD  
365 with increasing bias voltage. It is evident that at 1 V  $\mu\text{m}^{-1}$  the maximum CCD has  
366 not been reached in the case of S79 and S52. Nevertheless, to compare the measured  
367 data point with those provided by RD42, the CCD at 1  $\mu\text{m}$  has to be taken.

### 368 Irradiation damage factor

369 The irradiation damage factor  $k_\lambda$  is a way to quantify irradiation damage of a specific  
370 particle at a specific energy. Via this factor different types of irradiation can be  
371 compared. It is obtained experimentally by measuring the CCD of a number of  
372 samples at various irradiation steps and fitting the equation 1.5 to the data.  $\lambda$  is the  
373 measured CCD,  $\lambda_0$  is the CCD of a non-irradiated sample and  $\Phi$  the radiation dose.  
374 As a reference, the damage factor for 24 GeV protons is set to  $1 \times 10^{-18} \mu\text{m}^{-1} \text{ cm}^{-2}$ .

$$\frac{1}{\lambda} = \frac{1}{\lambda_0} + k_\lambda \cdot \Phi \quad (1.4)$$

$$\lambda = \frac{\lambda_0}{k_\lambda \lambda_0 \Phi + 1} \quad (1.5)$$

375 The data points with the maximum CCD obtained in the test beam measurements  
376 are plotted against radiation dose received in figure 1.7b. Equation 1.5 is fitted to  
377 the data points and a damage factor  $k_\lambda = (4.4 \pm 1.2) \times 10^{-18} \mu\text{m}^{-1} \text{ cm}^{-2}$  can be  
378 obtained. The value is for a factor of two higher than the damage factor obtained by  
379 RD42. This could be due to an insufficient priming time ahead of the measurement.  
380 In addition, the diamond samples have not been polished and re-metallised after  
381 irradiation, as is the case for the RD42. Also, with only two samples measured, the  
382 statistical uncertainty is high. Nevertheless, it can be concluded that the 300 MeV  
383 pions damage the diamond bulk significantly more than the 24 GeV protons.

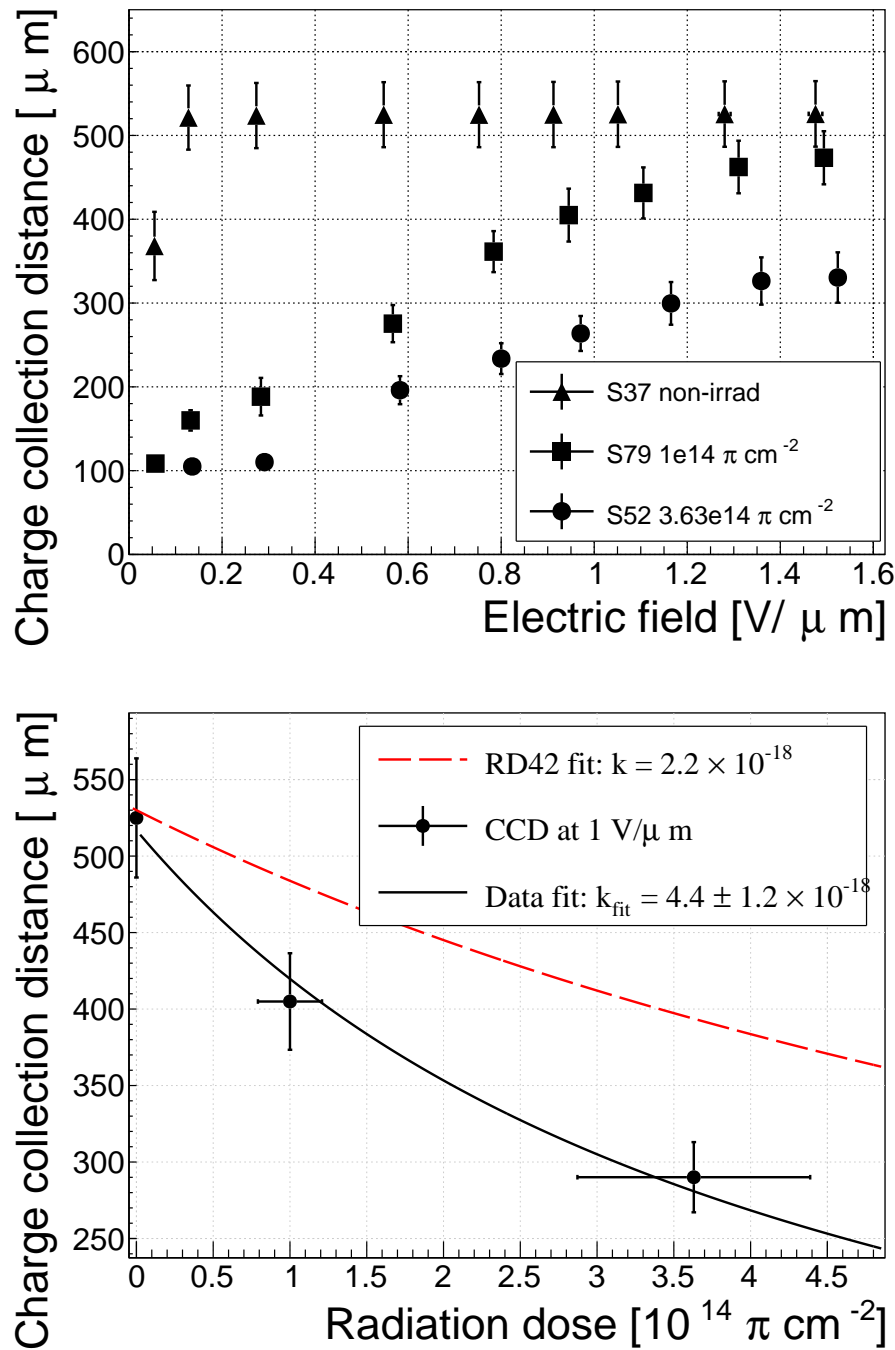


Figure 1.7: First figure shows the CCD for S37, S79 and S52 at a range of bias voltage settings. The charge collection distance at  $1 \text{ V}/\mu\text{m}$  bias voltage for the three diamond samples is then compared to the RD42 data for pion irradiation in the second figure. The data points are about 15–25 % lower than expected from the RD42 data [?].

<sup>385</sup> **1.3.2 Long-term measurement stability**

<sup>386</sup> An important requirement for particle detectors is a stable performance over long  
<sup>387</sup> periods of time. For instance, the charge collection for a defined radiation type and

388 quantity must not change over time or has to change in a predicted way. Diamonds  
389 are stable as long as their environment and their operating point does not change  
390 significantly. The stability of diamond detectors depends on many factors: material  
391 purity, polishing process, electrode material, irradiation damage etc. The aim is  
392 to study the behaviour of diamond under controlled conditions, with the goal to  
393 understand its limitations. One of these limitations is the received radiation dose as  
394 it can affect the long-term stability of the sensor during operation.

395 The three diamond samples (S37, S79 and S52) have been exposed to two different  
396 types of ionising radiation for a longer period to see if their behaviour changes over  
397 time. Two parameters have been observed in particular:

- 398     1. Charge collection of  $\beta$  particles and
- 399     2. Charge collection and ionisation profile of  $\alpha$  particles.

400 The results in this and in the following section show that priming plays an important  
401 role in improving the diamond measurement stability in both cases.

#### 402 $\beta$ long-term stability

403 The diamond samples have undergone a long-term stability test using  $\beta$  radiation.  
404 This has been done using a  $^{90}\text{Sr}$  source emitting  $\sim 2$  MeV electrons at a rate of  
405 approximately  $10^4 \text{ e}^- \text{ cm}^{-2}$ . To simulate the initial conditions in HEP experiments,  
406 the sensors must not be primed before starting the measurements. The measurement  
407 setup consists of a diamond sample (S37, S52 or S79) with the Cx spectroscopic  
408 amplifier, a silicon diode with a C6 amplifier for a trigger and a  $^{90}\text{Sr}$  source on top.  
409 A particle emitted by the source traverses the sensor bulk and hits the silicon diode,  
410 triggering the analogue signal readout. The source is left on the top for the course  
411 of the experiment. The measurements, however, are taken at discrete times. For  
412 every data point, approximately  $10^4$  triggers have to be recorded. The offline analysis  
413 of the recorded signal pulse amplitudes yields a landau distribution for every data  
414 point. The most probable value (MPV) of the distribution is proportional to the  
415 collected charge by the diamond sensor. The resulting graph of charge collection  
416 over time in figure 1.8 shows that the charge collection efficiency improves when the  
417 diamond sensor is primed with a  $\beta$  source. This is especially evident in the case of  
418 the two irradiated samples. S79 achieves close to a full efficiency whereas S52 reaches  
419 about 50 %. Both increases are significant. At a received dose of approximately  
420  $4 \times 10^6$  particles the signal stabilises. As expected, the signal of the non-irradiated S37  
421 does not change with priming – this pure sCVD diamond sample has the maximum  
422 collection distance from the start of the measurement.

423 The  $\sim 2.28$  MeV electrons emitted by this source are not MIPs; their charge depo-  
424 sition is higher than that of an electron MIP, according to the Bethe-Bloch distribu-  
425 tion [?]. Nevertheless, for the purpose of these measurements this energy is adequate  
426 since only the relative change in charge collection is of interest.

### 1.3. RADIATION LIMITATIONS

---

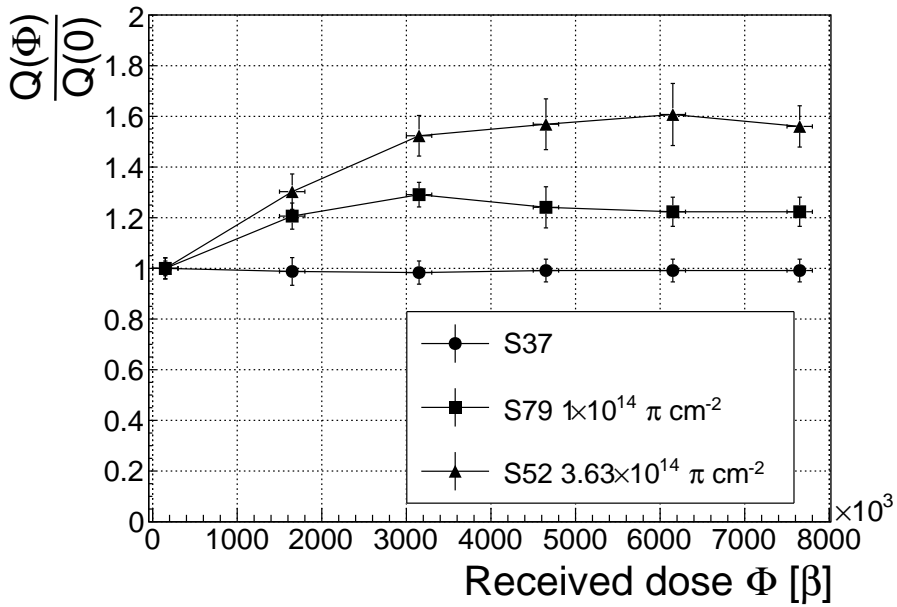


Figure 1.8: Relative increase of charge collection over time due to priming with the  $^{90}\text{Sr}$  radioactive source. The charge collection for the non-irradiated S37 stays constant. The bias voltage for this measurement is 1 V/ $\mu\text{m}$ .

To sum up, diamond is a good choice for  $\beta$  radiation detection. Even if damaged by radiation, it reaches a stable charge collection at a received dose of  $\sim 4 \times 10^6$  MIP particles. The efficiency decreases with a high irradiation dose (effects visible above  $10^{12}$  MIP  $\text{cm}^{-2}$ ). However, the decrease can be accounted for if the damage factor and the rate and energy of the particles are known.  $\gamma$  radiation has a similar impact on the diamond as the  $\beta$ . The incident photons, if they interact with the diamond, prime the bulk, increasing the charge collection efficiency. The difference, however, is that the interaction probability (cross-section) is lower for gammas [?, ?].

#### 435 $\alpha$ long-term stability

This part discusses the stability of irradiated diamond sensors during  $\alpha$  measurements. An  $^{241}\text{Am}$  source is used, emitting  $\alpha$  particles with a mean energy of 5.5 MeV. It is safe to assume that they affect the diamond differently than when subject to  $\beta$  radiation. This is due to the point-like charge carrier creation; an  $\alpha$  particle penetrates the bulk and stops at a depth of  $\sim 14$   $\mu\text{m}$  (for a 5.5 MeV particle). The deposited energy produces  $\frac{5.5 \text{ MeV}}{13.6 \text{ eV}} = 4 \times 10^5$  e-h pairs. Compared to a MIP, which produces an MPV of  $500 \mu\text{m} \times 36 \text{ e-h } \mu\text{m}^{-1} = 18 \times 10^3$  e-h pairs in a 500  $\mu\text{m}$ , the collected charge is for a factor of 22 higher. In addition, the energy is deposited in a small volume – 14  $\mu\text{m}$  in depth and  $\sim 20$  nm radially [?]. This dense distribution of charge carriers affects their behaviour at the start of the drift. Furthermore, carriers of only one polarity drift through the sensor while those of the opposite polarity almost instantly

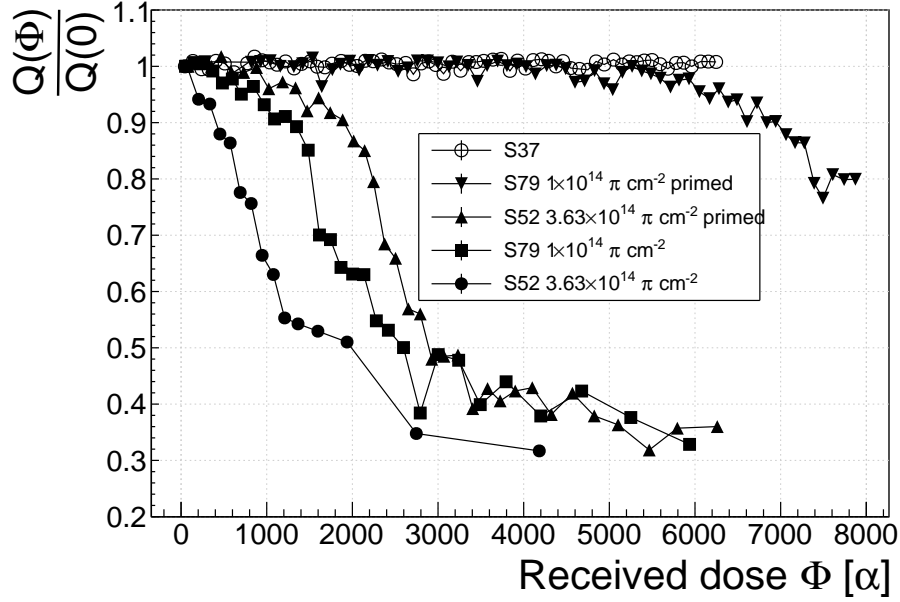


Figure 1.9: Relative decrease of collected charge with time for non-irradiated and irradiated diamond samples.

447 recombine with the adjacent electrode. Taking into account that the diamond bulk  
448 has been damaged by irradiation, these two phenomena might have an effect on the  
449 operation of the detector.

450 The first test has been carried out using the Cx spectroscopic amplifier, with  
451 the bias voltage of the samples set to +500 V. Figure 1.9 shows the results of 6500  
452 recorded hits at a rate of  $\sim 7$  particles per second. The collected charge  $Q(\Phi)$  for  
453 the non-irradiated sample is stable as compared to the initial collected charge  $Q(0)$   
454 (plotted as a relative value  $\frac{Q(\Phi)}{Q(0)}$ ). It is expected that the irradiated samples have  
455 a lower charge collection efficiency than the non-irradiated sample. However, their  
456 initial efficiency suddenly drops after a certain period of time. The initial efficiency  
457 after priming with  $\beta$  particles is higher than that without priming, but eventually it  
458 also deteriorates. In addition, the spread of measured energies increases significantly.  
459 Finally, the particle counting rate decreases with a decreased efficiency.

460 To investigate this sudden drop in efficiency, the current pulse shapes using a C2  
461 current amplifier have to be observed, as shown in figure 1.10. The shape of the  
462 pulse holds more information about the charge carrier properties in the sensor than  
463 solely the value of the integrated charge. This time only the primed S79 sample has  
464 been tested. Both the hole and the electron collection are observed to determine  
465 whether they behave differently or not. The sample has been measured long enough  
466 for the pulse shapes to start changing. The data in figures 1.10 show that the initially  
467 stable pulses start deteriorating – suddenly several different shapes start appearing,  
468 some still very similar to those from the beginning while the others with almost zero  
469 amplitude.

### 1.3. RADIATION LIMITATIONS

---

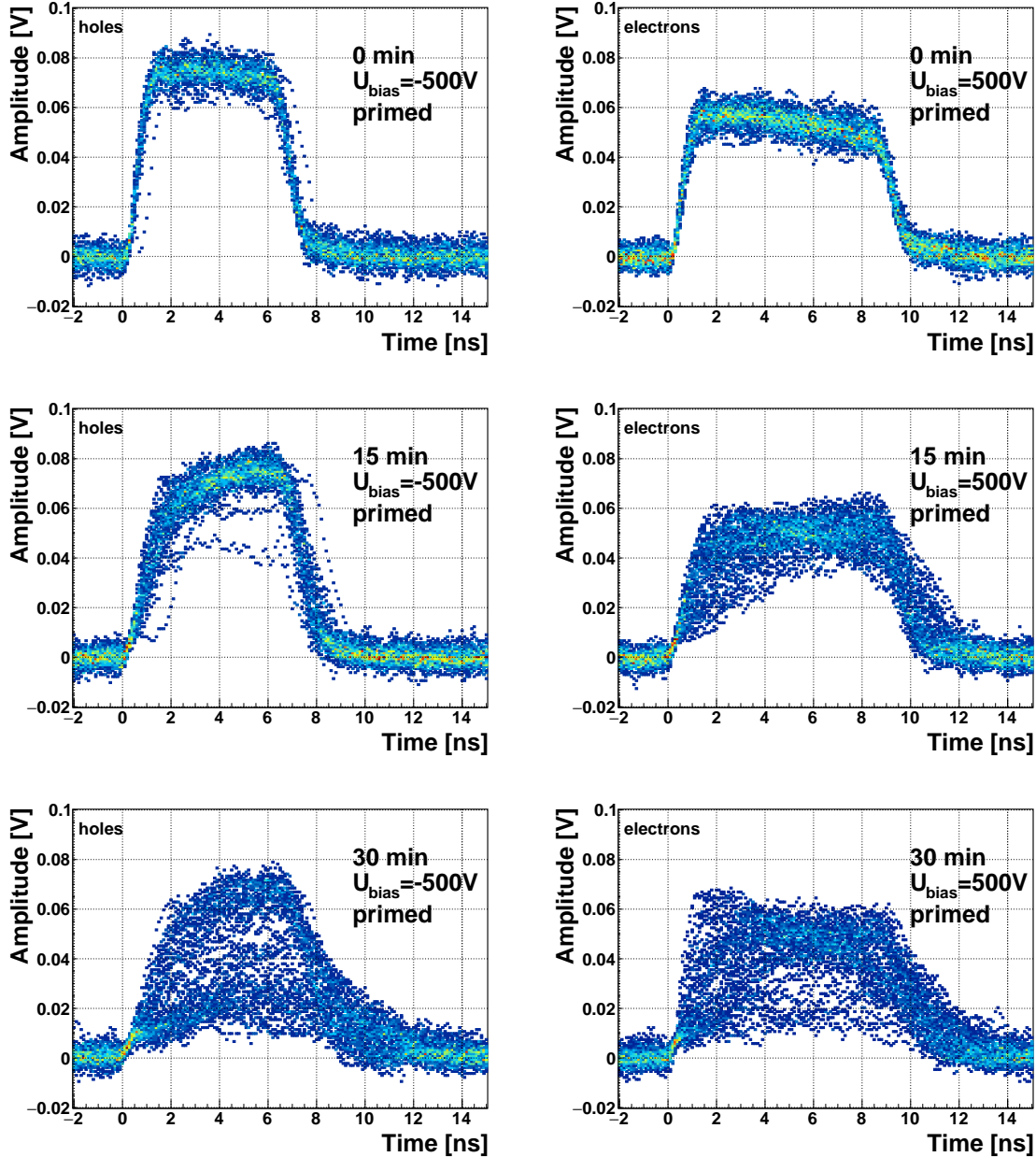


Figure 1.10: The signal of the irradiated and primed S79 deteriorates with time for both polarities. Every plot contains 60 superimposed pulses.

470 Some charges get stopped in the charge traps in the bulk for a long time, building  
 471 up regions of space charge. The built up space charge affects the electric field, making  
 472 it non-uniform. The non-uniform field in turn affects the drifting carriers, slowing  
 473 them down or speeding them up, depending on the field gradient. Since the movement  
 474 of the carriers is inducing the electric current, the field gradient can be observed in  
 475 the signal.

476 The second test with the C2 current amplifier has been carried out as follows: at

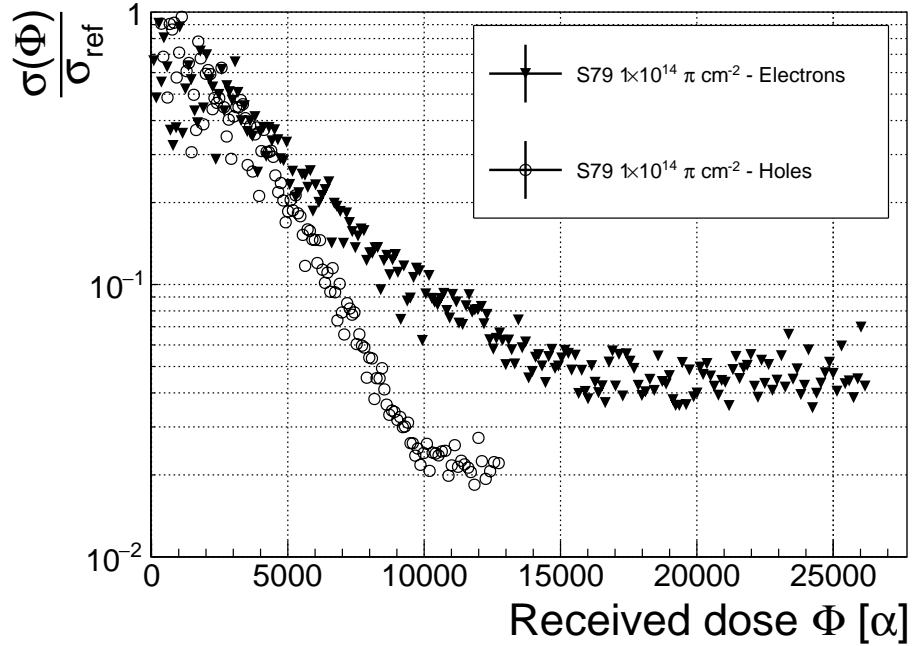


Figure 1.11: Deterioration of the pulse shapes with time.

477 the beginning of the test when the diamond is still operating stably, 60 pulses are  
 478 recorded. An average pulse is calculated. This is a reference pulse for the subsequent  
 479 measurement points. Then an RMS of the single pulses with respect to the reference  
 480 pulse is calculated and the resulting RMS values are summed together ( $\sigma_{\text{ref}}$ ).

481 All the subsequent data points also consist of a set of 60 pulses. At every data point  
 482 the summation of the RMS values of the individual pulses with respect to the initial  
 483 averaged pulse is calculated ( $\sigma$ ). The ratio between the initial  $\sigma_{\text{ref}}$  and discrete values  
 484  $\sigma$  gives a measure of change of the pulse shape with respect to the reference pulse at  
 485 the start of the measurement. Figure 1.11 shows the ratio  $\frac{\sigma_{\text{ref}}}{\sigma(\alpha \text{ dose})}$ . From the data  
 486 obtained it can be concluded that the initial pulse shape quickly starts deteriorating.  
 487 In fact, the deterioration of the shape follows an approximate exponential decay  
 488 function, which can be fitted to the data. The resulting decay constants for electrons  
 489 and holes are  $\tau_e = (4400 \pm 150) \alpha^{-1}$  and  $\tau_h = (3300 \pm 140) \alpha^{-1}$ . The electrons retain  
 490 the initial shape for longer. The deteriorated shapes also seem to be for a factor of 2  
 491 better than those of the holes.

492 **Restoring the pulse shapes** Finally, an effort has been made to find a way for the  
 493 pulse shapes to return to their initial state. Five methods are listed:

- 494 1. Removing the source and leaving the bias voltage switched on,
- 495 2. Removing the source and switching the bias voltage off,
- 496 3. Priming with  $\gamma$  at a rate of  $400 \text{ s}^{-1}\text{cm}^{-1}$  without applied bias voltage,
- 497 4. Priming with  $\beta$  at a rate of  $1000 \text{ s}^{-1}\text{cm}^{-1}$  with applied bias voltage and

## 1.4. TEMPERATURE LIMITATIONS

---

498 5. Priming with  $\beta$  at a rate of  $1000 \text{ s}^{-1}\text{cm}^{-1}$  without applied bias voltage.

499 The diamond sample S79 is first primed using a  $^{90}\text{Sr}$  source for about one hour.  
500 Then the bias voltage is switched on and an  $^{241}\text{Am}$  source is put on top. The pulses  
501 produced by the incident  $\alpha$  particles have a proper rectangular pulse at the beginning,  
502 but then start changing – first gradually and later increasingly more in an erratic way,  
503 as described in the text above. After approximately 30 minutes, one of the methods is  
504 tested. When a “healing” procedure is started, a set of 60 pulses is taken at irregular  
505 points of time to observe the change in the pulse shape and to assess the quality of the  
506 “healing” procedure. Then the bias voltage is switched off and the sample is primed  
507 again to reset its state before starting with the next run.

508 The results depicted in figure 1.12 show that the methods (3) and (5) improve the  
509 shape, method (2) helps slowly, (1) does not show any change with time and (4) at first  
510 improves, but then significantly degrades the shape. The effect observed in method  
511 (4) has already been described in [?]. The “healing” process therefore depends on the  
512 rate of radiation, the bias voltage and the time of exposure. The ionising radiation  
513 creates free charges, which quickly recombine close to the place of generation. It is  
514 likely that they also release the charges trapped during the measurement, reducing the  
515 overall effect of the space charge. The traps get filled with both flavours of carriers,  
516 thus they are neutralised. The pulse shape gradually returns to its initial state.

Procedure	Source	Bias voltage	Effectiveness
1	/	ON	no
2	/	/	slow
3	$^{60}\text{Co}$	/	YES
4	$^{90}\text{Sr}$	ON	no
5	$^{90}\text{Sr}$	/	YES

518 Table 1.2: Effectiveness of healing procedures.

519 In summary, the shape of the pulses caused by  $\alpha$  radiation changes with time  
520 for irradiated samples. The shape of the pulses gets distorted and becomes erratic.  
521 Charge collection decreases and its spread increases. This happens even faster for  
522 non-primed diamonds. To “heal” the diamond – to bring the pulse shapes back to  
523 their initial shape – the sample must be primed using a  $\beta$  or a  $\gamma$  source for several  
524 minutes at the bias voltage set to 0 V. Switching to the inverse polarity for a few  
525 seconds helps a bit, but in a long run distorts the signal, which cannot get back to  
526 its initial shape.

## 527 1.4 Temperature limitations

528 A test has been carried out to evaluate the effect of temperature changes on the  
529 output signal of the diamond sensors. A cryostat filled with liquid helium is used to  
530 cool down the sensor during the measurement process. The current signal response

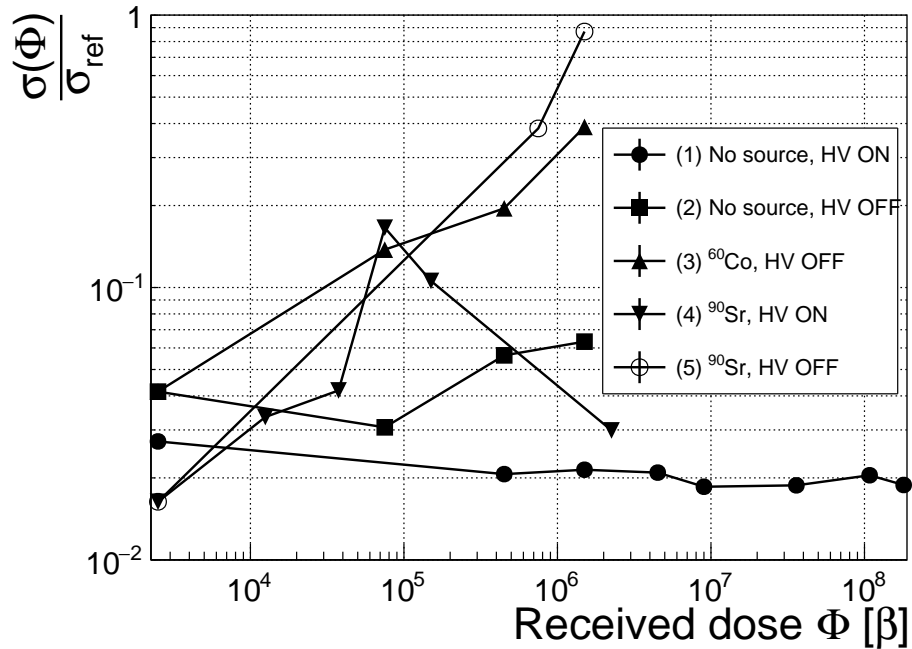


Figure 1.12: Comparison of the five procedures for the “healing” process for an irradiated diamond that had been exposed to  $\alpha$  radiation with a rate of  $10^1 \text{ s}^{-1}$ , with the bias voltage switched on, for at least 30 minutes.

531 to  $\alpha$ -particles is measured at 18 temperature points between 4 K and 295 K. At every  
 532 temperature point, a set of 300 pulses is read out at various bias voltages. Resulting  
 533 data show that the charge collection is stable down to 150 K, where it starts decreasing  
 534 and stabilises again at about one third of the initial value at 75 K. This behaviour  
 535 was first measured and discussed by H. Jansen [?].

536 The band gap energy in diamond is equal to  $E_g = 5.5 \text{ eV}$  while the average energy  
 537 to produce an electron-hole pair is  $E_{e-h} = 13.25 \text{ eV}$ . This means there is excessive  
 538 energy deposited in the diamond bulk. The incident  $\alpha$ -particle stops within  $\sim 10\text{--}15 \mu\text{m}$  of the bulk,  
 539 transferring all its energy to the lattice during deceleration. A  
 540 part of this energy directly ionises the carbon atoms, creating free electron-hole pairs.  
 541 The positively charged hole and the negatively charged electron in the hole attract  
 542 each other via the Coulomb force and may undergo a bonding process during which  
 543 a phonon is emitted.

544 The remaining energy, however, is converted into lattice vibrations (phonons [?,  
 545 ?]). This means that the lattice within the ionisation volume (approximately  $\sim 15 \mu\text{m} \times \sim 2 \text{ nm}$   
 546 in size) is briefly heated up. The hot plasma then cools down to the temperature of  
 547 the surrounding material by heat dissipation, (i.e. phonon transport). The free elec-  
 548 tron binds the free hole into a bound state (not recombination) – the exciton [?].  
 549 The exciton binding energy is 80 meV. At higher temperatures, the lattice provides  
 550 enough energy to excite the electron from the exciton state back to the conduction  
 551 band. At lower temperatures, however, the exciton lifetime increases, which means

## 1.4. TEMPERATURE LIMITATIONS

---

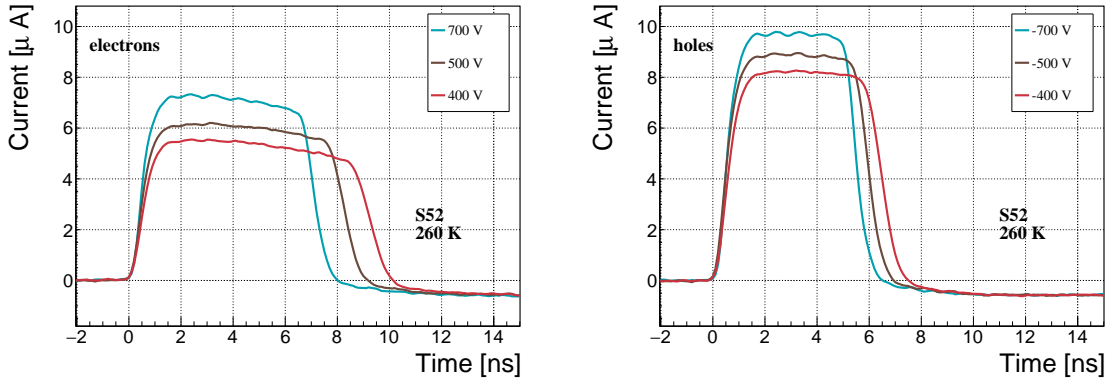


Figure 1.13: Varied bias voltage at a fixed temperature.

552 that it takes a longer time for the electrons to get re-excited to the conduction band.  
 553 The re-excitation lifetime at room temperature is  $\sim 30$  ps, increasing to  $\sim 150$   $\mu$ s at  
 554 50 K [?]. This means that some of the bound electrons do not even start drifting  
 555 within the period of  $\sim 10$  ns, which is the expected carrier drift time. When they  
 556 are finally freed, the current they induce is already hidden in the electronics noise.  
 557 The effective area of the observed current pulse is therefore smaller than that of a  
 558 pulse induced by all the carriers drifting at the same time. This in effect reduces the  
 559 measured collected charge. The longer the time constant, the lower the measured  
 560 collected charge, as shown in figure 1.17 below.

### 561 1.4.1 Temperature-variant $\alpha$ -TCT before irradiation

562 Three sCVD diamond samples have been tested at a range of temperatures using  
 563 the  $\alpha$ -TCT technique. At each temperature point, the bias voltage is set to several  
 564 positive and negative values. A set of 300 pulses is recorded at every data point  
 565 and averaged offline. The resulting averaged pulses of sample S37 at the 260 K  
 566 temperature point and a bias voltage of  $\pm 400$  V,  $\pm 500$  V and  $\pm 700$  V are shown in  
 567 figure 1.13. The pulses induced by holes as charge carriers are shorter than those  
 568 induced by electrons, which means that holes travel faster in diamond. The area of  
 569 the pulse, however, is the same for both polarities, which corresponds to the fact that  
 570 the same amount of charges is drifting in both cases.

571 Figure 1.14 shows pulses at a bias voltage set to  $\pm 500$  V across the range of  
 572 temperatures between 4 K and 295 K – room temperature (RT). Several conclusions  
 573 can be drawn by observing their shape. First, the pulse shapes change with decreasing  
 574 temperature. The pulse time gets shorter, hinting at the faster carrier drift velocity  
 575  $v_{\text{drift}}$ . Second, between 150 K and 75 K there is a significant change in shape - the  
 576 time constant of the rising edge increases significantly and the pulse area decreases.  
 577 From 75 K down to 4 K there is no significant observable change. Last, the top of  
 578 the pulse at the S52 is not flat, which means that a portion of the drifting charge is  
 579 lost along its way. This is due to charge trapping, likely by means of crystal defects

580 or impurities.

### 581 1.4.2 Temperature-variant $\alpha$ -TCT after irradiation

582 The irradiated S79 and S52 have been re-tested in the cryostat after irradiation. The  
583 aim was to observe how their pulse shapes change with decreasing temperature, in  
584 particular the decaying top of the pulses, as shown in figure 1.15. The decay time  
585 gives information on trapping of charge carriers while travelling through the diamond  
586 bulk. A variation of the decay time constant as a function of temperature might  
587 help to reveal the type and depth of the charge traps. To observe these effects or  
588 lack thereof, a number of requirements has to be met. First, the diamond samples  
589 are intentionally not primed prior to the experiment because priming would improve  
590 the pulse shapes and possibly change the decay time constant of the signal. Second,  
591 keeping in mind that the pulse shape of irradiated diamonds changes with time, the  
592 duration of the measurement of an individual data point has to be short – of the  
593 order of 30 seconds. Last, the sequence of the bias voltage settings is important, the  
594 reason for which is explained below.

595 Unfortunately it is not possible to avoid temporal pulse changes. For instance,  
596 one measurement point takes approximately one minute. After the measurement, the  
597 bias voltage polarity is swapped for a few seconds to bring the diamond back into its  
598 initial state. But a few seconds with respect to a minute is not enough. Therefore,  
599 when the bias voltage is set to the next value, there is still some residual effect of  
600 the previous measurement. Similar to the effects of polarisation, this effect is also  
601 decreasing the pulse height. This can be observed in figure 1.15, which shows the  
602 resulting pulses of S52 for bias voltages of  $\pm 200$  V,  $\pm 300$  V,  $\pm 400$  V and  $\pm 500$  V  
603 at 230 K and 260 K. In this case the measurements sequence is: 230K (200 V,  
604 300 V, 400 V, 500 V, -500 V, -400 V, -300 V), 260 K (-200 V, -300 V, -400 V, -  
605 500 V, 500 V, 400 V, 300 V). The changes in pulse shapes for holes at 230 K and  
606 260 K cannot be attributed to the temperature change. Instead, the explanation  
607 could lie in diamond “polarisation”. This means that, when exposed to an electric  
608 field with  $\alpha$  measurements ongoing, the diamond builds up an internal electric field  
609 of inverse polarity, which effectively reduces the overall electric field. This internal  
610 field does not dissipate when the external bias voltage is switched off. It can be  
611 said that the diamond becomes “polarised”. When switching the polarity of the  
612 external bias voltage, the internal and external electric field point in the same direction  
613 at the beginning, increasing the overall electric field and with it the pulse height.  
614 In figure 1.15, this happens when switching from 500 V (figure 1.15a) to -500 V  
615 (figure ??) at 230 K. The built up polarisation contributes to the pulse having a  
616 sharp rising edge and a high amplitude. This effect decays during the next two  
617 voltage points. There would be a handful of ways to avoid this polarisation effect in  
618 the data:

- 619 1. After every data point invert the bias voltage and leave it to return to a neutral  
620 state for the same amount of time,

#### 1.4. TEMPERATURE LIMITATIONS

---

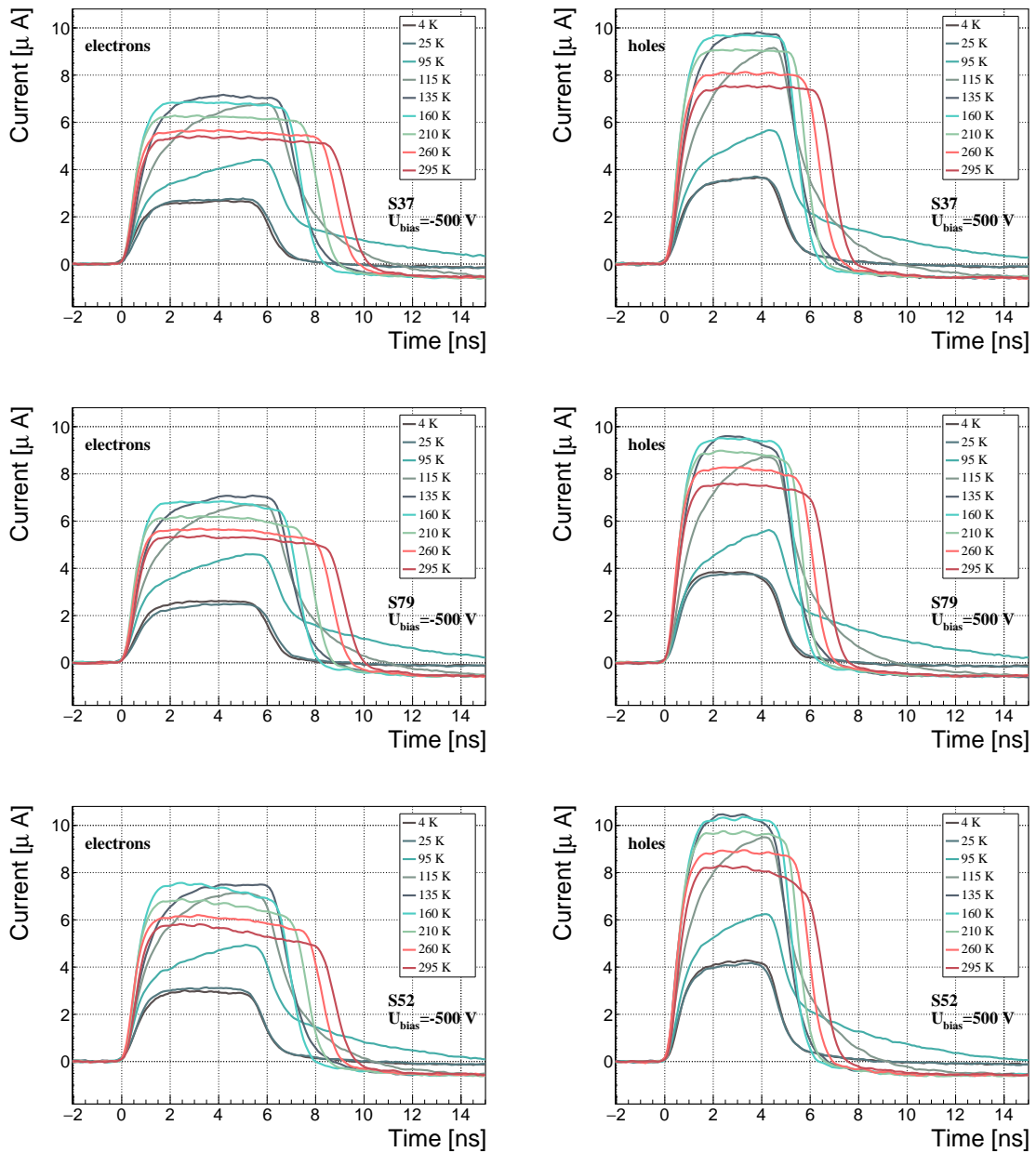


Figure 1.14: Several data points between 4 K and 295 K at a bias voltage of  $\pm 500$  V.

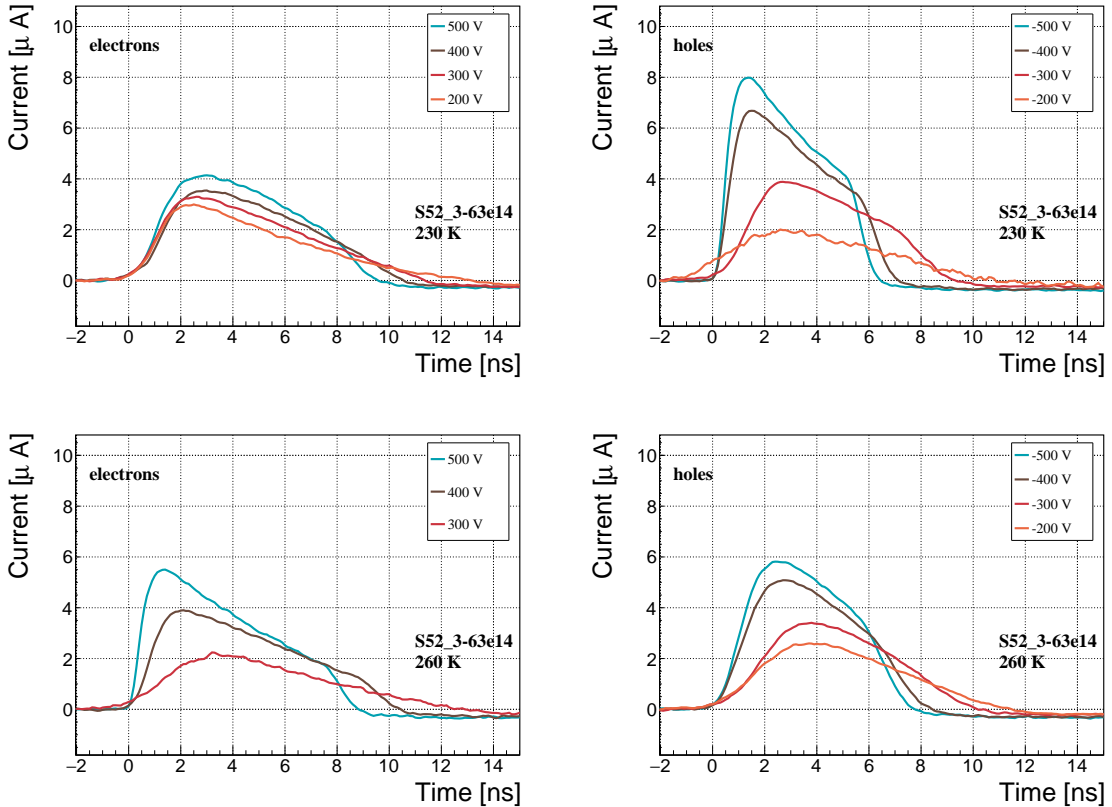


Figure 1.15: Varied bias voltage at a fixed temperature for an irradiated sample.

- 621     2. Make a hysteresis of data points, going from minimum negative to maximum
  - 622       positive bias several times,
  - 623     3. Reduce the measurement time at every bias voltage setting.
- 624     Unfortunately, options (1) and (2) are very time consuming and would increase the
- 625       overall experiment time to over one day. The third option would worsen the resulting
- 626       averaged pulses. In the end an alternative option was chosen: alternating the start-
- 627       ing bias voltage and the sequence at every temperature point. With this option, a
- 628       meaningful systematic error in analysing the pulse shapes can be attained.

629     Figure 1.16 shows the irradiated S52 and S79 as well as the non-irradiated S37

630       for comparison, all at a bias voltage of  $\pm 500$  V and at several temperature points

631       between 4 K and RT. It is evident that the radiation damage affected the shape of

632       the pulses across all temperatures.

### 633     **Collected charge as a function of temperature**

634     The area below the current pulse is proportional to the charge collected by the dia-

635       mond detector. The collected charge is observed as a function of temperature. First,

636       the amplitude values of the averaged pulses at a bias voltage of  $\pm 500$  V and across

## 1.4. TEMPERATURE LIMITATIONS

---

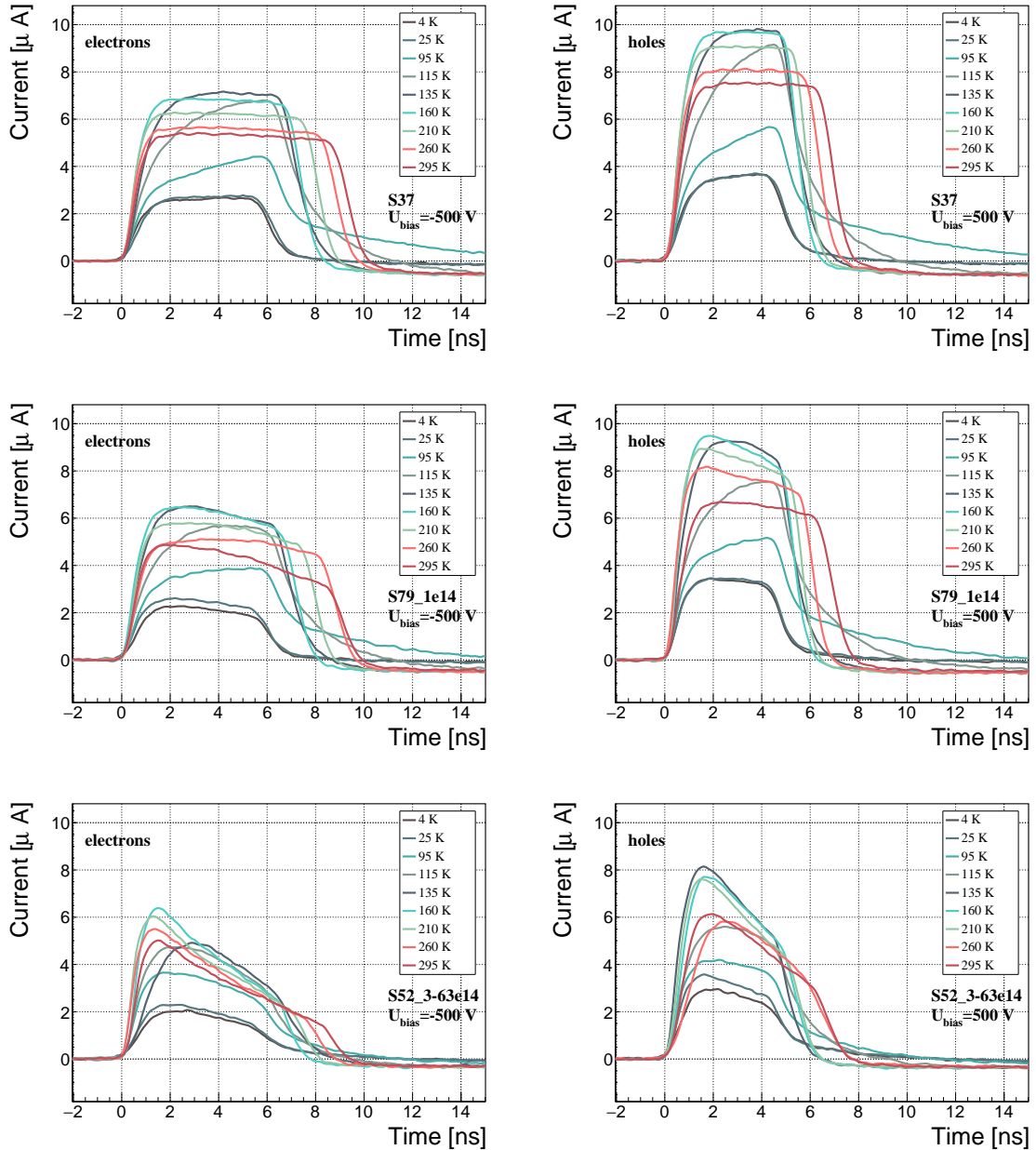


Figure 1.16: After irradiation: several data points between 4 K and 295 K at a bias voltage of  $\pm 500$  V.

the temperature range between 4 K and 295 K have to be integrated. Then a calibration factor is used to derive the charge for all data points. This factor is obtained using a Cx charge-sensitive amplifier. The resulting values for electrons and holes are plotted in figures 1.17a and 1.17b, respectively. Thesis [?] gives a model that explains the drop in charge below 150 K. The new contribution are the data points for the irradiated samples. The values for them are lower than the those of non-irradiated samples, which is expected.

644 The values for all samples are fairly stable in the range between 4 K and 75 K  
645 and between 150 K and 295 K. However, in the values for the irradiated S52 some  
646 excursions can be observed. This is due to the sequence of the measurement steps,  
647 which introduced a hysteresis effect and is explained in the preceding text.

648 The collected charge drops significantly from 150 K down to 75 K. In the non-  
649 irradiated samples the values in the lower temperature range are approximately 0.30  
650 of the values at the high range. For the irradiated ones this difference is lower – a  
651 factor of 0.35 for S79 and 0.5 for S52. An interesting detail is that the ratio between  
652 the values for non-irradiated samples and their irradiated counterparts at the lower  
653 range is different than at the higher range. Looking at the values for the electron  
654 collection in figure 1.17a: for S52 the lower ratio is equal to 1.28 and the higher equal  
655 to 1.7. For S79 these ratios are 1.00 and 1.09, which means that the difference in  
656 charge collection between 4 K and 75 K before and after irradiation is negligible.

### 657 Charge trapping

658 The carriers drifting through the bulk get stopped by the charge traps with a certain  
659 probability. This trapping happens uniformly throughout the diamond, decreasing  
660 the number of carriers in the charge cloud. Therefore the absolute number of trapped  
661 carriers decreases. At the same time the absolute number of trapped carriers per unit  
662 of length decreases. The resulting function for the number of drifting carriers per  
663 unit of length is a decaying exponential function:

$$I(t) = I(0) \cdot e^{-\frac{t-t_0}{\tau}} + I_0, \quad (1.6)$$

664 where  $I(0)$  is the initial induced current,  $I_0$  is the end current,  $t$  is time,  $t_0$  is temporal  
665 displacement of the pulse and  $\tau$  is the decay time constant. This value tells how long  
666 it takes before the amplitude of the pulse decreases to 63 % of its initial height.

667 The decaying exponential function has been fitted to the decaying top of the  
668 averaged pulses at bias voltages of  $\pm 400$  V and  $\pm 500$  V across all temperatures  
669 excluding the transitional range between 75 K and 150 K. The resulting decay time  
670 constants  $\tau$  for an individual temperature point are not equal, which stems from  
671 the fact that the pulses change with time due to “polarisation”. This counts as a  
672 systematic error. Therefore the fitted  $\tau$  for  $\pm 400$  V and  $\pm 500$  V are averaged into  
673 one value representing the measurement at that temperature point. Figure 1.18a  
674 shows the fitted  $\tau$  for the five samples between 4 K and 295 K. In principle, the  
675 time constants should be infinite for a perfect and non-irradiated sample. Here a  
676 slightly tilted top of the pulse due to space charge is already successfully fitted with  
677 an exponential function, resulting in a  $\tau$  of the order of  $(200 \pm 20)$  ns<sup>-1</sup>. Consequently  
678 the fitting method is not adequate for non-irradiated samples. For the irradiated  
679 samples, the fit becomes increasingly more meaningful. As seen in figure 1.18a, the  
680 fitted values of the irradiated samples are fairly stable across all temperatures. There  
681 is a slight increase in the decay time constant of the S52 from  $(6.0 \pm 0.5)$  ns<sup>-1</sup> above  
682 150 K to  $(8.5 \pm 0.9)$  ns<sup>-1</sup> below 75 K. On the other hand, this step is not observable

#### 1.4. TEMPERATURE LIMITATIONS

---

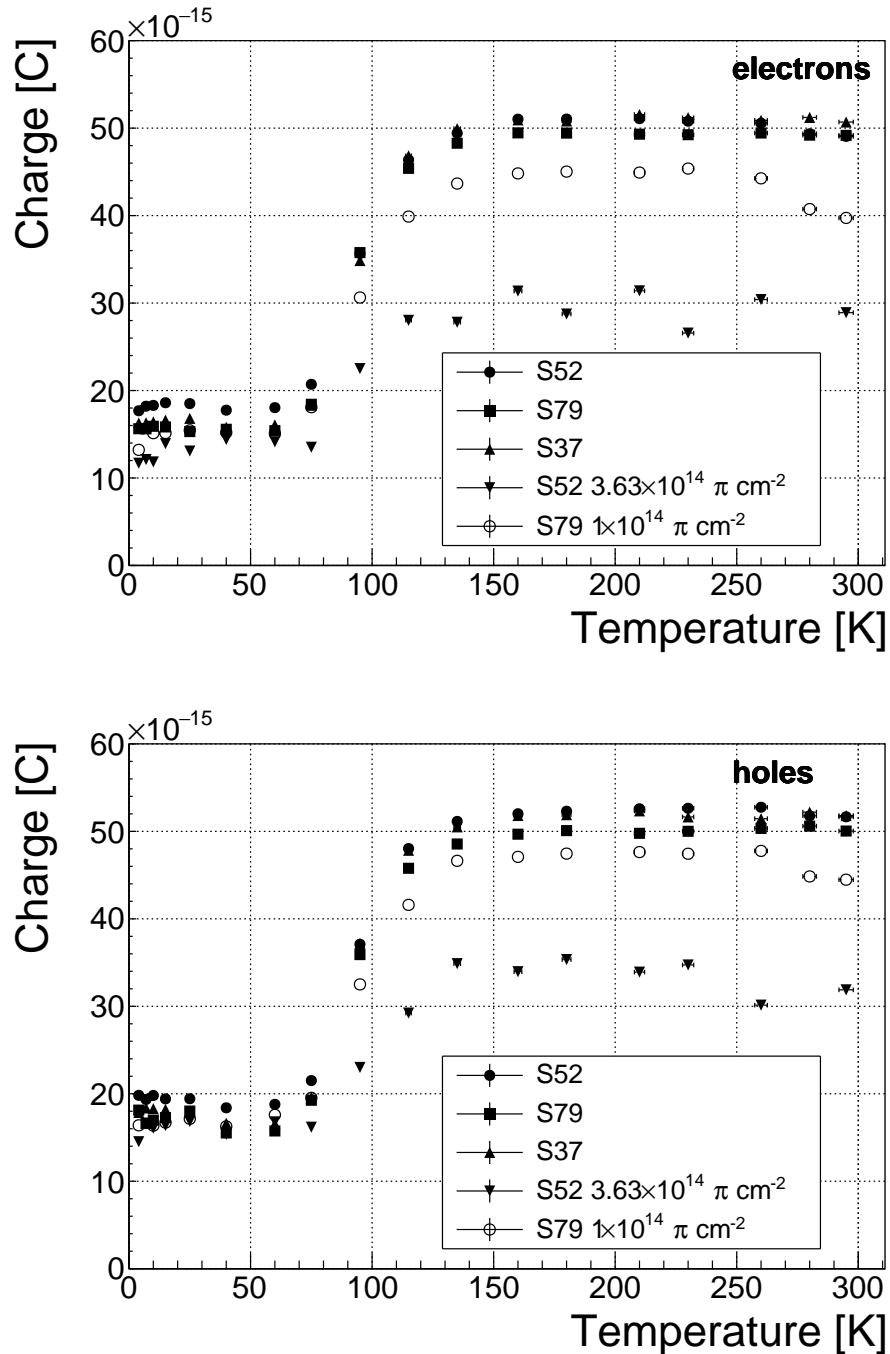


Figure 1.17: Collected charge as a function of temperature.

in the S79 data. With only one sample exhibiting this behaviour, the effect is not significant enough. Judging by the data acquired, the samples would need to be irradiated to doses above  $1 \times 10^{14} \pi \text{ cm}^{-2}$  to quantify this effect in detail. So far this effect is not regarded as significant for the scope of this thesis. Building on this assumption, the conclusion is that the signal decay time constant for irradiated sCVD

*CHAPTER 1. EXPERIMENTAL RESULTS*  
*DIAMOND IRRADIATION STUDY*

---

688 diamond is constant across the temperature range between 4 K and 195 K, excluding  
689 the transitional range between 75 K and 150 K.

690 Taking into account the conclusions above, all the values can be averaged into one  
691 decay constant. Figure 1.18b shows these values for all samples as a function of the  
692 received  $\pi_{300 \text{ MeV}}$  radiation dose. To estimate the carrier lifetime with respect to the  
693 radiation dose received, a similar model is used than that in section 1.5. This model  
694 states that the inverse of the carrier lifetime is linearly decreasing with increasing  
695 radiation dose:

$$\frac{1}{\tau} = \frac{1}{\tau_0} + \kappa_\tau \cdot \Phi \quad (1.7)$$

696

$$\tau = \frac{\tau_0}{\kappa_\tau \tau_0 \Phi + 1} \quad (1.8)$$

697 where  $\tau_0$  is the lifetime for a non-irradiated sample (real lifetime, therefore of the order  
698 of  $400 \text{ ns}^{-1}$ ),  $\tau$  is the lifetime of an irradiated sample,  $\Phi$  is the received radiation dose  
699 and  $\kappa_\tau$  the lifetime degradation factor. For these data the fitted factor is equal to  
700  $\kappa_\tau = (3.6 \pm 0.8) \times 10^{-16} \text{ s cm}^2 \pi_{300 \text{ MeV}}^{-1}$ . Using this factor, the steepness of the decay  
701 in the pulse shape with respect to radiation dose can be estimated. This can help  
702 when designing a system where current pulse shape is an important factor.

#### 1.4. TEMPERATURE LIMITATIONS

---

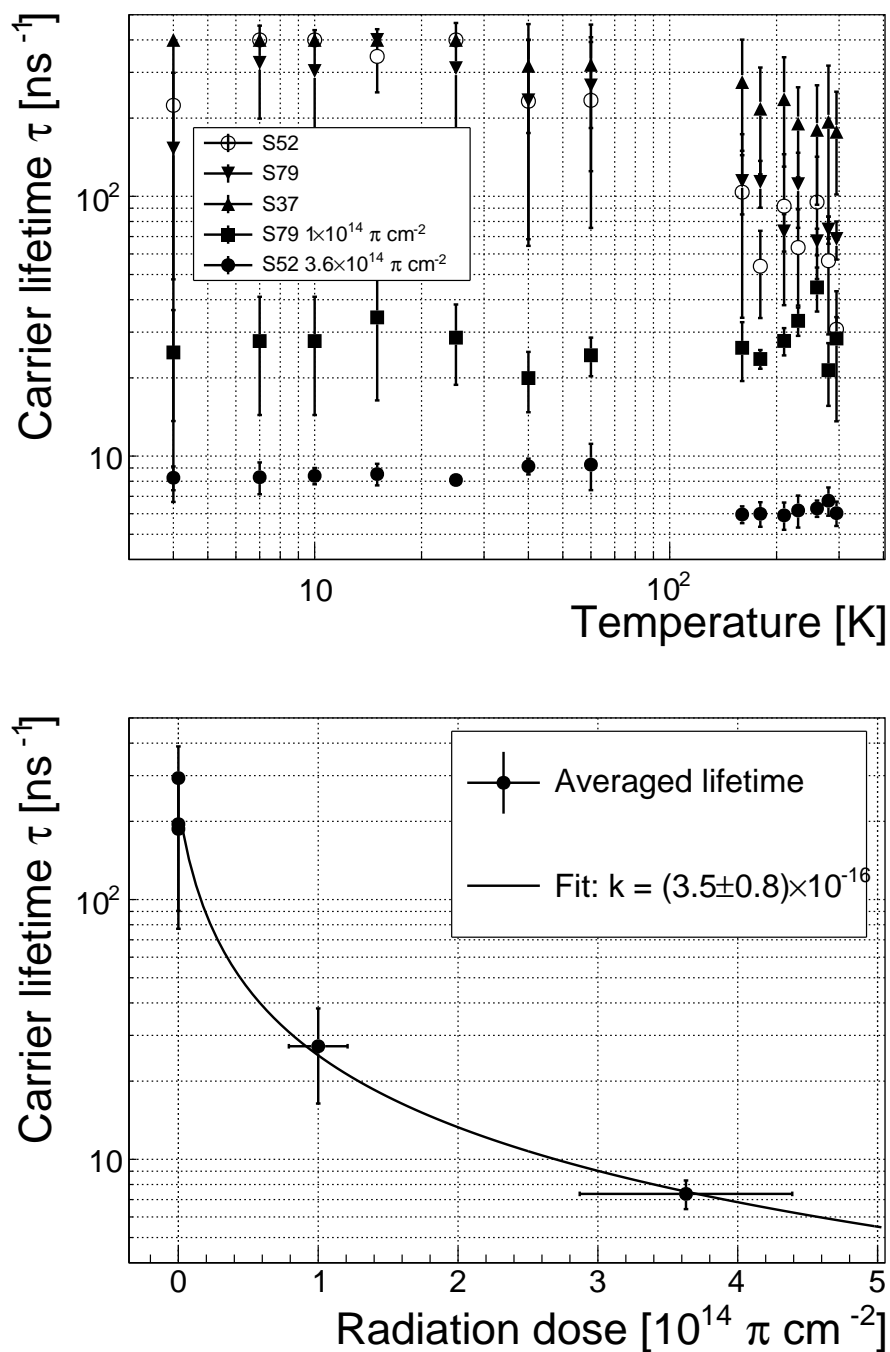


Figure 1.18: Charge carrier lifetime decreases with irradiation, but is stable across the range of temperatures between 4 K – 75 K and 150 K – 295 K. The first figure shows the carrier lifetime  $\tau$  as a function of temperature whereas the second figure depicts the carrier lifetime averaged over all temperatures and plotted against the  $\pi$  irradiation dose.

703 **1.5 Conclusion**

704 This chapter gives an overview of the capabilities and limitations of diamond as  
705 a particle detector. Three effects on diamond were studied – noise, radiation and  
706 temperature, the focus being on the latter two.

707 Two sCVD diamond detectors were irradiated with 300 MeV pions. They were  
708 tested alongside a non-irradiated sample to observe the changes in the ability to detect  
709  $\alpha$ ,  $\beta$  and  $\gamma$  radiation. Their charge collection efficiency was measured in a test beam  
710 facility using . The results were compared to the results from the RD42 collaboration  
711 and a DPA model. A radiation damage factor  $k_\lambda = (3.0 \pm 1.0) \times 10^{-18} \mu\text{m}^{-1} \text{cm}^{-2}$  was  
712 obtained for  $\pi_{300 \text{ MeV}}$  particles. The data point was not in agreement with the data  
713 provided by RD42 nor with the model. However, the irradiation process and the low  
714 number of tested samples hold a relatively high statistical uncertainty. In addition,  
715 there was no diamond surface treatment done in between the measurements, as is  
716 the case in the study conducted by RD42. The results obtained in the course of  
717 these measurements are going to be fed into the existing pool of data in the RD42  
718 collaboration.

719 The next step was to test the long-term capabilities for  $\alpha$  detection. The shape  
720 of the ionisation profile was investigated to determine the behaviour of the charge  
721 carriers in the irradiated diamond. An exponential decay was observed in the pulses  
722 of irradiated samples, proving that there are charge traps in the bulk that were created  
723 during irradiation. Then a long-term stability test was carried out. The results show  
724 that the irradiated diamond detectors do not provide a stable and reliable long-term  
725 measurement of  $\alpha$  particles. This might be due to a space-charge build-up in the  
726 bulk, which changes the electric field, affecting the charge carriers. A procedure to  
727 improve the pulse shape using  $\beta$  and  $\gamma$  radiation was proposed.

728 Finally, the diamond sensors were cooled down to temperatures between 4 K and  
729 295 K. Their response to  $\alpha$  particles was observed. The results of the non-irradiated  
730 and irradiated samples were compared. The effect of reduction for the number of  
731 drifting charges due to exciton recombination was observed in both sets of data.  
732 The second set had a superimposed effect of charge trapping during the drift, which  
733 was represented by an exponential decay in the signal. The decay time constant  
734 did not change with temperature. Therefore all temperature points for individual  
735 samples were averaged and the decay time constants were plotted against the received  
736 radiation dose. A damage factor equal to  $\kappa_\tau = (3.5 \pm 0.8) \times 10^{-16} \text{ s cm}^2 \pi_{300 \text{ MeV}}^{-1}$  for  
737 non-primed diamonds was defined.